Available online at www.sciencedirect.com
ScienceDirect
Journal of Computational Physics 225 (2007) 2214–2248
JOURNAL OF COMPUTATIONAL PHYSICS
www.elsevier.com/locate/jcp

A relaxation-projection method for compressible flows. Part II: Artificial heat exchanges for multiphase shocks

Fabien Petitpas [a], Erwin Franquet [a], Richard Saurel [a,b,*], Olivier Le Metayer [a]

[a] *Polytech'Marseille, Université de Provence and SMASH Project UMR CNRS 6595 – IUSTI-INRIA, 5 rue E. Fermi, 13453 Marseille Cedex 13, France*

[b] *University Institute of France and SMASH Project UMR CNRS 6595 – IUSTI-INRIA, 5 rue E. Fermi, 13453 Marseille Cedex 13, France*

Received 17 November 2006; received in revised form 7 March 2007; accepted 19 March 2007
Available online 30 March 2007

Abstract

The relaxation-projection method developed in Saurel et al. [R. Saurel, E. Franquet, E. Daniel, O. Le Metayer, A relaxation-projection method for compressible flows. Part I: The numerical equation of state for the Euler equations, J. Comput. Phys. (2007) 822–845] is extended to the non-conservative hyperbolic multiphase flow model of Kapila et al. [A.K. Kapila, Menikoff, J.B. Bdzil, S.F. Son, D.S. Stewart, Two-phase modeling of deflagration to detonation transition in granular materials: reduced equations, Physics of Fluids 13(10) (2001) 3002–3024]. This model has the ability to treat multi-temperatures mixtures evolving with a single pressure and velocity and is particularly interesting for the computation of interface problems with compressible materials as well as wave propagation in heterogeneous mixtures. The non-conservative character of this model poses however computational challenges in the presence of shocks. The first issue is related to the Riemann problem resolution that necessitates shock jump conditions. Thanks to the Rankine–Hugoniot relations proposed and validated in Saurel et al. [R. Saurel, O. Le Metayer, J. Massoni, S. Gavrilyuk, Shock jump conditions for multiphase mixtures with stiff mechanical relaxation, Shock Waves 16 (3) (2007) 209–232] exact and approximate 2-shocks Riemann solvers are derived. However, the Riemann solver is only a part of a numerical scheme and non-conservative variables pose extra difficulties for the projection or cell average of the solution. It is shown that conventional Godunov schemes are unable to converge to the exact solution for strong multiphase shocks. This is due to the incorrect partition of the energies or entropies in the cell averaged mixture. To circumvent this difficulty a specific Lagrangian scheme is developed. The correct partition of the energies is achieved by using an artificial heat exchange in the shock layer. With the help of an asymptotic analysis this heat exchange takes a similar form as the 'pseudoviscosity' introduced by Von Neumann and Richtmyer [J. Von Neumann, R.D. Richtmyer, A method for the numerical calculation of hydrodynamic shocks, J. Appl. Phys. 21 (1950) 232–237]. The present Lagrangian numerical scheme thus combines Riemann solvers and artificial heat exchanges. An Eulerian variant is then obtained by using the relaxation-projection method developed earlier by the authors for the Euler equations. The method is validated against exact solutions based on the multiphase shock relations

DOI of original article: 10.1016/j.jcp.2006.10.004.
* Corresponding author. Address: Polytech'Marseille, Université de Provence and SMASH Project UMR CNRS 6595 – IUSTI-INRIA, 5 rue E. Fermi, 13453 Marseille Cedex 13, France. Tel.: +33 9 128 8511; fax: +33 9 128 8322.
E-mail address: Richard.Saurel@polytech.univ-mrs.fr (R. Saurel).

0021-9991/$ - see front matter
doi:10.1016/j.jcp.2007.03.014

as well as exact solutions of the Euler equations in the context of interface problems. The method is able to solve interfaces separating pure fluids or heterogeneous mixtures with very large density ratio and with very strong shocks.

Keywords: Interfaces; Shocks; Multiphase flows; Relaxation

0. Introduction

The multiphase flow model of Kapila et al. [13] presents nice features regarding acoustic propagation in dense granular materials as well as its ability to solve interface problems separating compressible fluids [3,21] by using the same algorithm and equations everywhere (interfaces, mixtures and pure fluids). This model involves five partial differential equations in the context of two fluids: two equations for the masses, one equation for the mixture momentum, one equation for the mixture energy and a non-conservative equation for the volume fraction. With this approach, the mixture evolves under a unique pressure and velocity but remains in non-equilibrium regarding thermal and chemical effects. These non-equilibrium effects can be used to model chemical reactions and phase transformations [28].

Multiphase mixtures evolving under unique pressure and velocity are involved in many practical applications dealing with shock propagation into solid alloys, solid and liquid energetic materials, specific composite materials, etc. Such mixtures evolve under a single pressure and velocity as mechanical relaxation effects are stiff. Kapila et al. [13] model is obtained as the asymptotic limit of the Baer and Nunziato [5] non-equilibrium model in the presence of stiff mechanical relaxation.

One of the main features of these hyperbolic multiphase flow models rely in their ability to solve interfaces separating compressible fluids or mixtures of compressible fluids. During the last decade, many algorithms have been developed in order to solve interface problems between compressible fluids by using the same numerical strategy everywhere. Some of them use single pressure and velocity approaches [1,3,4,10,14,20–22,26,30]. Other methods deal with several pressures and velocities [2,6,16,23–25].

The present work deals with the numerical approximation of Kapila et al. [13] model as it is an interesting candidate to model extra physics such as phase transition, capillary effects, combustion etc. Such effects are easier to model and analyze in the context of a single velocity flow model. However, the first difficulty is related to the non-conservative character of this model and to the computation of shocks into mixtures.

Kapila et al. [13] model assumes isentropic evolution of the phases. It thus requires closure relations in the presence of shocks. Corresponding Rankine–Hugoniot jump conditions are obtained in a companion paper [27]. They are able to provide excellent predictions for shock propagation into mixtures when stiff velocity and pressure relaxation effects are present. These relations have been validated against experiments for more than 100 tests in the same reference, and over a larger set of experimental data by Trunine [34]. With the help of these relations, exact and approximate Riemann solvers are built.

However, the Riemann problem solution is not sufficient to obtain a reliable numerical scheme. This is again due to the presence of a non-conservative equation. Indeed, a conventional average for a non-conservative variable such as the volume fraction has no physical sense. This difficulty is first illustrated with Godunov [12] method where convergence errors are reported.

Thus another method is developed. It is based on the Lagrangian resolution of the system with the help of internal energy equations for the phases. The pressure averages that appear in these non-conservative equations are determined in order to respect energy conservation and to mimic the shock relations given in Saurel et al. [27]. However, the numerical diffusion of the shock front results in a thermodynamic path for the phases that is inconsistent with the one imposed in the exact solution. Consequently, the method no longer converges to the exact solution in the presence of strong shocks.

To reach convergence the method has to deal with the energy or entropy partition in the different phases. This energy partition has to agree with the one of the exact solution, imposed by the Rankine–Hugoniot conditions. In order to match this partition, the flow model is complemented by heat exchanges. An asymptotic analysis of these exchanges enables their formulation as differential terms, involving the velocity divergence.

Following [36] such terms can be used in the shock layer only. By making appropriate calibration of the heat exchange coefficient (or its asymptotic analogue) accurate results are obtained with correct energy partition.

The last step is to project the solution in order to obtain an Eulerian scheme. Conventional projection is inappropriate due to the presence of non-conservative variables. Thus, the relaxation-projection method of Saurel et al. [26] is extended to the context of the multiphase model.

The paper is organized as follows.

The single velocity and single pressure multiphase flow model of Kapila et al. [13] is presented in Section 1. The Riemann invariants and shocks relations of Saurel et al. [27] are used to derive exact and approximate 2-shocks Riemann solvers.

A conventional Godunov method is developed with the approximate solver in Section 2. Convergence difficulties that occur at shock front are illustrated.

In Section 3 a Lagrangian method is developed on the basis of the energy equations of the phases. The pressure average involved in the numerical integration of these equations is determined in order to fulfill energy conservation and to mimic the shock relations of Saurel et al. [27]. Again this method does not converge to the exact solution. This is due to the numerical smearing of the shock front where it does not appear possible to impose the correct thermodynamic path.

In Section 4 a correction to the previous method is developed. It relies on extra terms of the model, related to heat exchanges. An asymptotic analysis is carried out in order to express these relaxation terms as differential ones. Doing so, heat exchange takes the form of artificial viscosity, which can be used in the shock layer only. Under proper calibration of the heat exchange coefficient, the method provides results of high accuracy and remains very robust.

In Section 5 the relaxation-projection method of Saurel et al. [26] is extended to project the solution onto the Eulerian grid.

1. Multiphase flow model and Riemann solvers

We consider the single pressure and velocity multiphase flow model of Kapila et al. [13]:

$$
\begin{aligned}
&\frac{\partial \alpha_1}{\partial t} + u\frac{\partial \alpha_1}{\partial x} = \frac{\rho_2 c_2^2 - \rho_1 c_1^2}{\frac{\rho_1 c_1^2}{\alpha_1} + \frac{\rho_2 c_2^2}{\alpha_2}}\frac{\partial u}{\partial x},\\
&\frac{\partial (\alpha\rho)_1}{\partial t} + \frac{\partial (\alpha\rho)_1 u}{\partial x} = 0,\\
&\frac{\partial (\alpha\rho)_2}{\partial t} + \frac{\partial (\alpha\rho)_2 u}{\partial x} = 0,\\
&\frac{\partial (\rho u)}{\partial t} + \frac{\partial (\rho u^2 + p)}{\partial x} = 0,\\
&\frac{\partial (\rho E)}{\partial t} + \frac{\partial (\rho E u + p u)}{\partial x} = 0,
\end{aligned}
\tag{1.0}
$$

where $\rho = (\alpha\rho)_1 + (\alpha\rho)_2$ denotes the mixture density, $\rho E = \rho e + \rho\frac{u^2}{2} = (\alpha\rho)_1 e_1 + (\alpha\rho)_2 e_2 + \rho\frac{u^2}{2}$ denotes the mixture total energy per unit volume, and α_k the volume fraction of phase k.

The internal energies of the phases $e_1 = e_1(p, \rho_1),\ e_2 = e_2(p, \rho_2)$ are given by the equations of state (EOS) of each phase. The sound speeds of the phases c_1 and c_2 are also functions of pressure and phase's density.

This model can be obtained by different methods. The first one consists in the determination of the asymptotic model, in the limit of stiff mechanical relaxation, of the non-equilibrium model of Baer and Nunziato [5]. This method was used by Kapila et al. [13]. The second method consists in expressing under differential form the pressure equilibrium condition $p_1(\rho_1, s_1) = p_2(\rho_2, s_2)$ under the constraints that phases entropies (s_1 and s_2) conserve along phase trajectories [21]. This model expresses the behavior of a two phase mixture that evolves under a unique pressure and velocity but with two temperatures and entropies. It is of interest for the computation of wave propagation in mixtures of condensed materials, as well as for the computation of interface problems separating pure fluids and interfaces separating mixtures.

For the sake of simplicity, it is assumed that each phase is governed by the stiffened gas (SG) EOS:

$$p_k(\rho_k, e_k) = (\gamma_k - 1)\rho_k e_k - \gamma_k p_{\infty k}, \quad k = 1, 2. \tag{1.1}$$

The application of the mixture energy definition and pressure equilibrium condition results in a mixture EOS of SG type (1.2) that closes system (1.0):

$$p(\rho, e, \alpha_1, \alpha_2) = \frac{\rho e - \left(\frac{\alpha_1 \gamma_1 p_{\infty 1}}{\gamma_1 - 1} + \frac{\alpha_2 \gamma_2 p_{\infty 2}}{\gamma_2 - 1}\right)}{\frac{\alpha_1}{\gamma_1 - 1} + \frac{\alpha_2}{\gamma_2 - 1}}. \tag{1.2}$$

Obviously, other options are possible but the SG EOS is sufficient for the present developments.

In this section an exact Riemann solver for system (1.0) is built from which an approximate 2-shocks solver is deduced. This solver is then used in the Godunov method to illustrate computational difficulties at shock fronts.

1.1. Exact Riemann solver

1.1.1. Basic relations

The multiphase flows model (1.0) is hyperbolic with the following characteristic velocities: $u - c_w$, $u + c_w$ and u, where c_w is the equilibrium mixture sound velocity [37] defined by $\frac{1}{\rho c_w^2} = \frac{\alpha_1}{\rho_1 c_1^2} + \frac{\alpha_2}{\rho_2 c_2^2}$. The structure of the Riemann problem associated to this model involves three waves and four different configurations (vacuum appearance is excluded of the present analysis). The jump relations through the various waves must be determined to obtain the intermediate states.

(a) *Riemann invariants*

A different formulation of the system (1.0) is used in this part. The set of unknowns is now composed of the mixture density ρ, the velocity u, the mass fraction of one of the phases Y_1 and the entropy of each phase s_1 and s_2. This leads to the next system:

$$\begin{aligned}
&\frac{\partial \rho}{\partial t} + u\frac{\partial \rho}{\partial x} + \rho\frac{\partial u}{\partial x} = 0,\\
&\frac{\partial u}{\partial t} + u\frac{\partial u}{\partial x} + \frac{1}{\rho}\frac{\partial p}{\partial x} = 0,\\
&\frac{\partial Y_1}{\partial t} + u\frac{\partial Y_1}{\partial x} = 0,\\
&\frac{\partial s_1}{\partial t} + u\frac{\partial s_1}{\partial x} = 0,\\
&\frac{\partial s_2}{\partial t} + u\frac{\partial s_2}{\partial x} = 0.
\end{aligned} \tag{1.3}$$

For the Riemann invariants determination, the different variables are expressed in the form: $W(x,t) = \tilde{W}(\varsigma)$, with $\varsigma = x - \sigma t$, σ being an arbitrary wave speed. It does imply $\frac{\partial W}{\partial t} = -\sigma\frac{\mathrm{d}\tilde{W}}{\mathrm{d}\varsigma}$ and $\frac{\partial W}{\partial x} = \frac{\mathrm{d}\tilde{W}}{\mathrm{d}\varsigma}$. Thus, system (1.3) becomes:

$$\begin{aligned}
&(u - \sigma)\frac{\mathrm{d}\rho}{\mathrm{d}\varsigma} + \rho\frac{\mathrm{d}u}{\mathrm{d}\varsigma} = 0,\\
&(u - \sigma)\frac{\mathrm{d}u}{\mathrm{d}\varsigma} + \frac{1}{\rho}\frac{\mathrm{d}p}{\mathrm{d}\varsigma} = 0,\\
&(u - \sigma)\frac{\mathrm{d}Y_1}{\mathrm{d}\varsigma} = 0,\\
&(u - \sigma)\frac{\mathrm{d}s_1}{\mathrm{d}\varsigma} = 0,\\
&(u - \sigma)\frac{\mathrm{d}s_2}{\mathrm{d}\varsigma} = 0.
\end{aligned} \tag{1.4}$$

System (1.4) is now used to determine the different Riemann invariants, through the rarefaction waves as well as contact surfaces.

(b) *Interface conditions*

Interface conditions determination is obvious from system (1.4) as this wave propagates at the fluid velocity $\sigma = u$. That leads to:

$$\begin{aligned} &[u] = 0, \\ &[p] = 0 \end{aligned} \tag{1.5}$$

with the notation $[f] = f_R - f_L$, the jump of any function f between a right state (R) and a left state (L).

(c) *Rarefaction waves*

Rarefaction waves propagate at speed $\sigma = u \pm c_w$. The Riemann invariants through such waves are:

$$\begin{aligned} &\mathrm{d}p = \pm \rho c_w \, \mathrm{d}u, \\ &\mathrm{d}p = c_w^2 \, \mathrm{d}\rho, \\ &\mathrm{d}Y_1 = 0, \\ &\mathrm{d}s_1 = 0, \\ &\mathrm{d}s_2 = 0. \end{aligned} \tag{1.6}$$

Signs + and − correspond respectively to right- and left-facing waves. Note that the second invariant is redundant with the two last ones. Indeed, the mixture entropy invariant reads $\mathrm{d}s = \sum_k Y_k \, \mathrm{d}s_k = 0$ and implies $\mathrm{d}p = c_w^2 \, \mathrm{d}\rho$.

By using the SG EOS for each phase, the two last equations of system (1.6) are integrated yielding:

$$\rho_k = \rho_k^0 \left(\frac{p + p_{\infty k}}{p^0 + p_{\infty k}} \right)^{\frac{1}{\gamma_k}}, \quad k = 1, 2. \tag{1.7}$$

The first equation of system (1.6) involves the mixture acoustic impedance ρc_w. With the present mixture EOS (1.2) it only depends on the pressure and is given by the following expression:

$$\rho c_w = \left(\sum_k \frac{Y_k}{\rho_k^2 c_k^2} \right)^{-\frac{1}{2}} = \left(\sum_k \frac{Y_k^0}{\rho_k^{0\,2} c_k^{0\,2} \left(\frac{p + p_{\infty k}}{p^0 + p_{\infty k}} \right)^{\frac{\gamma_k + 1}{\gamma_k}}} \right)^{-\frac{1}{2}}. \tag{1.8}$$

Unfortunately, the first equation of system (1.6) with (1.8) cannot be integrated analytically. A numerical integration method will be used to obtain the corresponding variation. The details will be given in the next subsection.

(d) *Shock relations*

Except regarding the first equation of system (1.0) that expresses under non-conservative form, jump conditions are available for the other equations:

$$\begin{aligned} &(\alpha\rho)_k^* (u^* - \sigma) = (\alpha\rho)_k^0 (u^0 - \sigma), \\ &\rho^* u^* (u^* - \sigma) + p^* = \rho^0 u^0 (u^0 - \sigma) + p^0, \\ &\rho^* (u^* - \sigma) E^* + p^* u^* = \rho^0 (u^0 - \sigma) E^0 + p^0 u^0, \end{aligned} \tag{1.9}$$

where σ represents the shock velocity and the superscripts '0' and '*' correspond, respectively, to pre- and post-shock states.

These equations can also be written as:

$$\begin{aligned} &Y_k^* = Y_k^0, \\ &\rho^* (u^* - \sigma) = \rho^0 (u^0 - \sigma) = m, \\ &p^* - p^0 + m^2 (v^* - v^0) = 0, \\ &e^* - e^0 + \frac{p^* + p^0}{2} (v^* - v^0) = 0, \end{aligned} \tag{1.10}$$

where the mass fraction is given by: $Y_k = \alpha_k \rho_k / \rho$. The mixture internal energy is defined by $e = Y_1 e_1 + Y_2 e_2$ and the mixture specific volume reads $v = Y_1 v_1 + Y_2 v_2$ (where $v_k = 1/\rho_k$). The closure of system (1.10) necessitates an extra relation. In a companion paper [27] an appropriate kinetic relation is proposed. We summarize hereafter the basis of this analysis.

- The theoretical analysis starts with observations of shock layers in multiphase mixtures computed with the seven equations non-equilibrium multiphase flow model [5] in the presence of mechanical relaxation. For sufficiently weak shock waves, it is shown that the two-phase shock has a smooth profile, and that at each point of this layer, the two phases have nearly the same velocity and pressure. This behavior is explained by a dispersion mechanism due to relaxation effects and to the differences in the frozen sound speed of the phases. This last feature allows acoustic waves of the post-shock state to cross the shock front. This feature is absent in single phase flows and results here in a smooth shock layer.
- As the shock layer is smooth and mechanical equilibrium assumption valid at each point of this layer, integration between pre- and post-shock states is simplified. Rather than considering the integration of a non-equilibrium model with seven partial differential equations [5] involving relaxation and non conservative terms, it is possible to consider its asymptotic limit with stiff pressure and velocity relaxation. In this context, the two energy equations of the seven equation model after asymptotic analysis reduce to:

$$\alpha_k \left(\rho_k \frac{\mathrm{d}e_k}{\mathrm{d}t} + p \frac{\partial u}{\partial x} \right) = -p \frac{\mathrm{d}\alpha_k}{\mathrm{d}t}, \quad \text{or} \quad \frac{\mathrm{d}e_k}{\mathrm{d}t} + p \frac{\mathrm{d}v_k}{\mathrm{d}t} = 0, \quad \text{or} \quad \frac{\mathrm{d}s_k}{\mathrm{d}t} = 0 \tag{1.11}$$

  with, $e_k = e_k(p, \rho_k)$. It is interesting to note that the drag work is absent in the first form of Eqs. (1.11) while the pressure work $(-p\frac{\mathrm{d}\alpha_k}{\mathrm{d}t})$ is still present. It means that drag contribution to the evolution of internal energy is negligible in this limit. In general, integration of any formulation of the phase's energy equations (1.10) has the potential to provide a kinetic relation. However, the choice of the energy equation form and the way it is integrated has importance as developed hereafter.
- Two main options are possible with the integration of (1.11).
  - *Constant entropy relation*
    Integration of the third form of (1.11) results in:

$$s_k^* = s_k^0. \tag{1.12}$$

    However, if such a choice is done for each phase k, the energy conservation in (1.10) is violated. Another option is possible. It consists in using (1.12) for one of the phases only while preserving energy conservation. Such option is:
    * Inaccurate when compared to experimental data.
    * Not symmetric. This may have serious consequences when dealing with an arbitrary number of fluids.
    * Inconsistent with the single phase limit. Indeed the model must deal with arbitrary concentrations in particular when solving interface problems.

    The option (1.12) is thus rejected.
  - *Hugoniot type relation*
    It consists in integrating the second differential form of Eqs. (1.11). Expressed in the shock wave frame under steady flow assumption it reads:

$$\frac{\mathrm{d}e_k}{\mathrm{d}x} + p \frac{\mathrm{d}v_k}{\mathrm{d}x} = 0.$$

    Its integration between pre- and post-shock states reads:

$$\int_{-\infty}^{+\infty} \frac{\mathrm{d}e_k(x)}{\mathrm{d}x}\, \mathrm{d}x + \int_{-\infty}^{+\infty} p(x) \frac{\mathrm{d}v_k(x)}{\mathrm{d}x}\, \mathrm{d}x = 0.$$

    It can be written as:

$$e_k^* - e_k^0 + \hat{p}_k \int_{-\infty}^{+\infty} \frac{\mathrm{d}v_k(x)}{\mathrm{d}x}\, \mathrm{d}x = 0 \tag{1.13}$$

with

$$\hat{p}_k = \frac{\int_{-\infty}^{+\infty} p(x) \frac{\mathrm{d}v_k(x)}{\mathrm{d}x}\,\mathrm{d}x}{\int_{-\infty}^{+\infty} \frac{\mathrm{d}v_k(x)}{\mathrm{d}x}\,\mathrm{d}x} = \frac{\int_{-\infty}^{+\infty} p(x) \frac{\mathrm{d}v_k(x)}{\mathrm{d}x}\,\mathrm{d}x}{v_k^* - v_k^0}.$$

A relation between the various pressure averages $\hat{p}_1$ and $\hat{p}_2$ may be found. Indeed, the pressure average of phase 1 can be written as:

$$\hat{p}_1 = \frac{\int_{-\infty}^{+\infty} p(x) \frac{\mathrm{d}v_1}{\mathrm{d}v_2} \frac{\mathrm{d}v_2(x)}{\mathrm{d}x}\,\mathrm{d}x}{v_1^* - v_1^0}. \tag{1.14}$$

As shown in Saurel et al. [27], for a given shock speed, $\frac{\mathrm{d}v_1}{\mathrm{d}v_2}$ is nearly constant inside the shock layer. Therefore, $\frac{\mathrm{d}v_1}{\mathrm{d}v_2}$ is approximated as:

$$\frac{\mathrm{d}v_1}{\mathrm{d}v_2} = \frac{v_1^* - v_1^0}{v_2^* - v_2^0}. \tag{1.15}$$

Note that this approximation is necessarily valid for weak shocks. By inserting this approximation into (1.14) we get:

$$\hat{p}_1 = \frac{\int_{-\infty}^{+\infty} p(x) \frac{\mathrm{d}v_2(x)}{\mathrm{d}x}\,\mathrm{d}x}{v_2^* - v_2^0} = \hat{p}_2 = \hat{p}.$$

It means that both pressure averages are equal. Eq. (1.13) now becomes

$$e_k^* - e_k^0 + \hat{p}(v_k^* - v_k^0) = 0. \tag{1.16}$$

In this equation the pressure average $\hat{p}$ has to be determined. This average is of capital importance: all differences between different thermodynamic paths rely in the estimate for this average. This average must be compatible with the energy conservation in (1.10), written in the form:

$$e^* - e^0 + \bar{p}(v^* - v^0) = 0$$

for which the pressure average is unambiguously known: $\bar{p} = (p^* + p^0)/2$.

By using the mixture internal energy and specific volume definitions, the mixture energy equation becomes:

$$Y_1(e_1^* - e_1^0 + \bar{p}(v_1^* - v_1^0)) + Y_2(e_2^* - e_2^0 + \bar{p}(v_2^* - v_2^0)) = 0.$$

Replacing in this equation the phase's internal energy variations with (1.16) we get:

$$Y_1(\bar{p} - \hat{p})(v_1^* - v_1^0) + Y_2(\bar{p} - \hat{p})(v_2^* - v_2^0) = 0.$$

That is:

$$(\bar{p} - \hat{p})(v^* - v^0) = 0.$$

As the specific volume varies across a shock wave, the energy conservation implies: $\hat{p} = \bar{p}$. And the phase's internal energy jumps read:

$$e_k^* - e_k^0 + \frac{p^* + p^0}{2}(v_k^* - v_k^0) = 0. \tag{1.17}$$

Relation (1.17) is the kinetic relation that closes system (1.10). We note that:

* It corresponds to the Hugoniot relation for each phase.
* By construction it preserves conservation of the total energy.
* It is in agreement with the single phase limit.
* It preserves symmetry.
* It guarantees volume fraction positivity.
* It is shown in Saurel et al. [27] that the mixture Hugoniot is tangent to the mixture isentrope.
* It has been validated for more than 100 tests involving shocks with 12 different mixtures. These relations were proposed independently by Trunine [34] and validated against 230 tests involving 23 different mixtures. The predictions of (1.10) with (1.17) always showed excellent agreement with the experiments.

A convenient form of these jump conditions when used into a Riemann solver is obtained by expressing the various variables as functions of the post-shock pressure. When the phases are governed by the SG EOS (1.1) the system reads:

$$\begin{aligned} &u = u^0 \pm m(v^0 - v),\\ &p = p^0 + m^2(v^0 - v),\\ &Y_k = Y_k^0,\\ &\rho_k^H = \rho_k^0 \frac{(\gamma_k+1)(p+p_{\infty k}) + (\gamma_k-1)(p^0+p_{\infty k})}{(\gamma_k-1)(p+p_{\infty k}) + (\gamma_k+1)(p^0+p_{\infty k})}, \quad k = 1,2. \end{aligned} \tag{1.18}$$

The signs + and − in the first equation correspond, respectively, to right- and left-facing waves. In these relations the shock mass flow rate m of the mixture appears. As the mixture specific volume is only function of pressure ($v(p) = \sum_k \frac{Y_k}{\rho_k^H(p)}$), the shock mixture mass flow rate only depends on the pressure too: $m = \sqrt{\frac{p-p^0}{v^0-v(p)}}$.

1.1.2. Algorithm

All the necessary relations to solve the Riemann problem shown in Fig. 1 are now available. It is noticeable that whatever the wave considered, the jump relations depend only on the pressure.

Depending on the value of pressure p^* two cases are to be considered:

- If $p* > p^0$, a shock wave is present and system (1.18) is used to obtain the solution behind this wave.
- If $p* \leqslant p^0$, a rarefaction wave is present and the Riemann invariants (1.8) are used.

The material velocity can always be written in the form $u = u^0 \pm \Phi(p)$ with $\Phi(p) = \frac{(p-p^0)}{m}$ for a shock wave and $\Phi(p) = \int_{p^0}^{p} \frac{\mathrm{d}p}{\rho c_w}$ for a rarefaction wave, where the sign + (−) corresponds to the right- (left-) facing wave.

A numerical integration is necessary to compute $\Phi(p) = \int_{p^0}^{p} \frac{\mathrm{d}p}{\rho c_w}$. The Gauss–Legendre method is used:

$$\int_{p^0}^{p} \frac{\mathrm{d}p}{\rho c_w} = \frac{p-p^0}{2} \sum_{k=1}^{n} \omega_k \frac{1}{\rho c_w(x_k)} \tag{1.19}$$

with:

$$x_k = \frac{p+p^0}{2} + \frac{p-p^0}{2}\xi_k, \quad \xi_k \in [-1;1], \quad x_k \in [p^0;p], \tag{1.20}$$

where ω_k and ξ_k are the values of the Gauss–Legendre coefficients. A six points approximation is accurate enough in the present applications.

Whatever the wave pattern considered, the velocity is then determined by:

$$\begin{aligned} &u_{\mathrm{L}}^* = u_{\mathrm{L}} - \Phi_{\mathrm{L}}(p^*),\\ &u_{\mathrm{R}}^* = u_{\mathrm{R}} + \Phi_{\mathrm{R}}(p^*). \end{aligned} \tag{1.21}$$

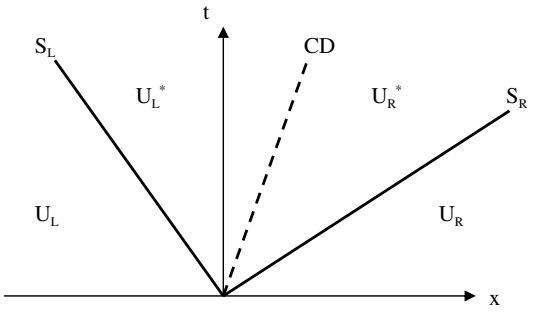

Fig. 1. Structure of the Riemann problem. The left- and right-facing waves (S_{L} and S_{R}) are either shock or rarefaction waves.

At the contact surface the second interface condition must be fulfilled ($u_L^* = u_R^* = u^*$). Eqs. (1.21) are combined to obtain a single equation only depending on the pressure p^*.

$$f(p^*) = u_R^* - u_L^* = u_R - u_L + \Phi_L(p^*) + \Phi_R(p^*) = 0. \tag{1.22}$$

Eq. (1.22) is nonlinear and is solved by the Newton–Raphson method. Reaching the solution p^*, the velocity u^* is then calculated thanks to one of the relations (1.21). The remaining flow variables are determined by relations (1.8) or (1.18) according to the wave's type.

1.1.3. Examples and validations

1.1.3.1. An interface separating almost pure fluids. In this part, the accuracy of the exact solver is checked in a limit case. An interface separates two almost pure fluids. Because the fluids are almost pure, the multiphase Riemann problem solution must converge to the Euler equations solution and a direct comparison is then possible.

A tube of 1 m long contains two chambers separated by an interface at the location $x = 0.8$ m. Each chamber contains a mixture of water and air. The initial density of the water is $\rho_{water} = 1000\ kg\ m^{-3}$ and the EOS parameters are $\gamma_{water} = 4.4$ and $P_{\infty,water} = 6 \times 10^8$ Pa. The initial density of air is $\rho_{air} = 10\ kg\ m^{-3}$ and EOS parameters are $\gamma_{air} = 1.4$ and $P_{\infty,air} = 0$ Pa. The left chamber contains a very small volume fraction of air $\alpha_{air} = 10^{-6}$ and the pressure is equal to 10^9 Pa. The right chamber contains the same fluids but the volume fractions are reversed. The pressure is equal to 10^5 Pa. In both chambers the velocity is equal to $0\ m\ s^{-1}$.

The exact solutions of the single phase Euler equations and the multiphase flow model (1.0) are compared in Fig. 2 at time $t = 220$ μs.

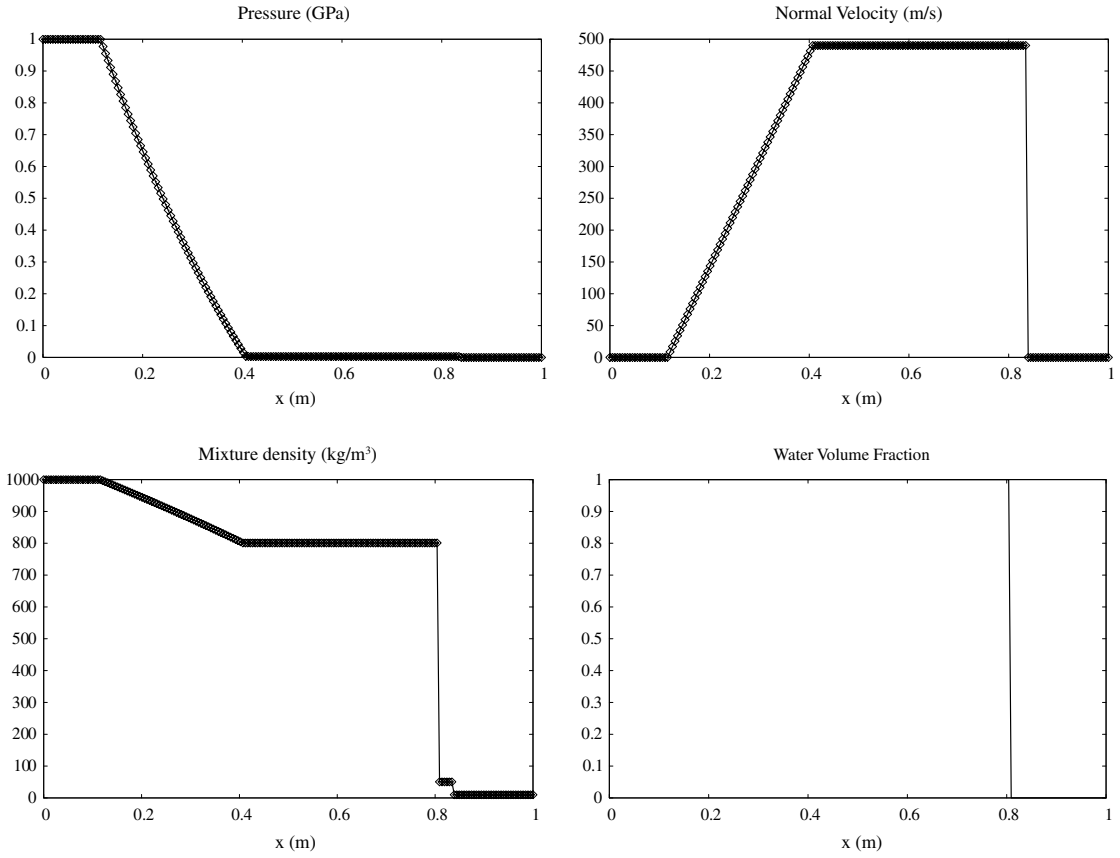

Fig. 2. Liquid/gas shock tube. Comparison of the exact two-phase solver (solid line) and exact Euler solver (symbols). In the single phase limit, the two solutions are merged. The volume fraction is not compared because it is absent in the Euler equations.

1.1.3.2. A shock tube problem involving two mixtures. A one meter length tube contains two chambers separated by an interface at the location $x = 0.6$ m. The same mixture made of epoxy and spinel fills the left and right chambers. The initial density of the epoxy is $\rho_{\text{epoxy}} = 1185\ \text{kg m}^{-3}$ and its EOS parameters are $\gamma_{\text{epoxy}} = 2.43$ and $P_{\infty,\text{epoxy}} = 5.3 \times 10^9$ Pa. The spinel has an initial density equal to $\rho_{\text{spinel}} = 3622\ \text{kg m}^{-3}$ and is characterized by $\gamma_{\text{spinel}} = 1.62$ and $P_{\infty,\text{spinel}} = 141 \times 10^9$ Pa.

The initial volume fractions in both chambers are: $\alpha_{\text{epoxy}} = 0.5954$ ($\alpha_{\text{spinel}} = 1 - \alpha_{\text{epoxy}}$). This value corresponds to the one used in the experiments recorded in the book of Marsh [18]. The pressure at the left of

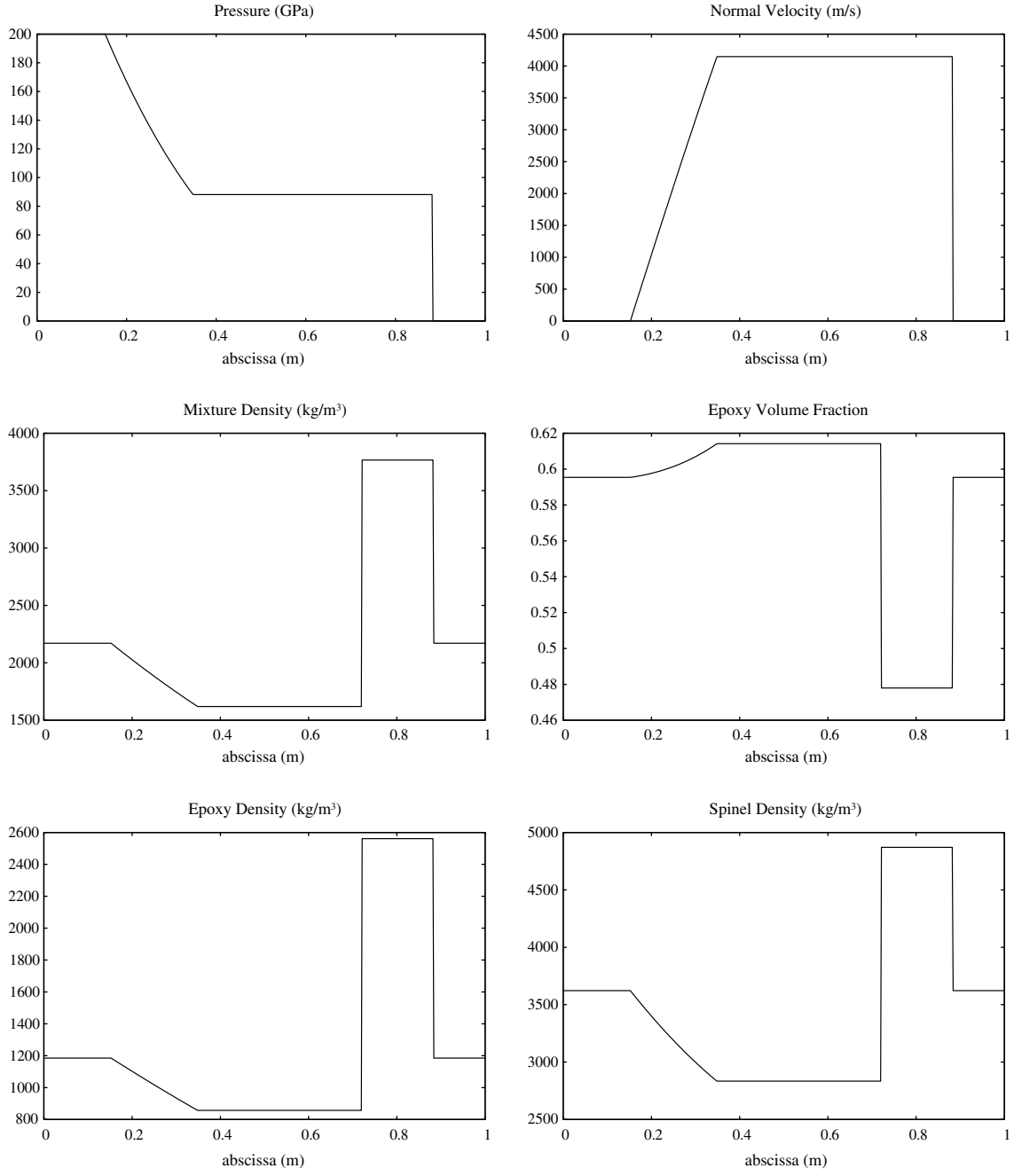

Fig. 3. Epoxy–spinel shock tube. This solution will serve as reference for the numerical scheme that will be developed.

the interface is equal to 2×10^{11} Pa, while the pressure in the right chamber is equal to 10^5 Pa. All the materials are initially at rest. The solution at time $t = 29$ μs is shown in Fig. 3.

1.2. Approximate Riemann solver

In this part a 2-shocks approximate solver is developed. The main drawback with the previous exact solver is related to the Riemann invariants that require a numerical integration. It implies several difficulties:

- The computation of sonic points is expensive.
- It prevents from a general use of the model. Indeed, with general EOS the numerical values of the acoustic impedance (1.9) at the integration points will have to be first computed: the roots of the nonlinear function linking the density and the pressure have to be determined. Then the Riemann invariant can be computed. The computational cost is thus considerably increased.

These remarks restrict the choice for the method to treat rarefaction waves. All rarefaction waves will be treated as rarefaction 'shocks' with relations (1.18). Let us examine the reasons why this is a reasonable choice:

- The Rankine–Hugoniot relations (1.18) are algebraic and guarantee conservation.
- It was shown in Saurel et al. [27] that the mixture Hugoniot curve and isentrope are tangent: for small variations the Hugoniot curve and isentrope are merged.

The approximate Riemann solver is thus a 2-shocks solver [33] and the algorithm is simplified.
The pressure at the contact surface is obtained by solving the non-linear equation:

$$f(p^*) = u_R^* - u_L^* = u_R - u_L + \frac{p^* - p_R}{m_R} + \frac{p^* - p_L}{m_L} \tag{1.23}$$

with the same definitions as in (1.18).
The solution is reached with the Newton–Raphson method. Once the pressure p^* is obtained, the remaining flow variables are determined with (1.18). This approximate solver will be used in the various numerical schemes examined in the rest of the paper.

2. A conventional Godunov type method

We examine in this section the simplest way to project the flow variables onto the computational cell. For the sake of simplicity a Lagrangian version of the Godunov method is considered. A schematic view of the wave's propagation into a Lagrangian cell is shown in Fig. 4.
Only two waves enter the Lagrangian cell:

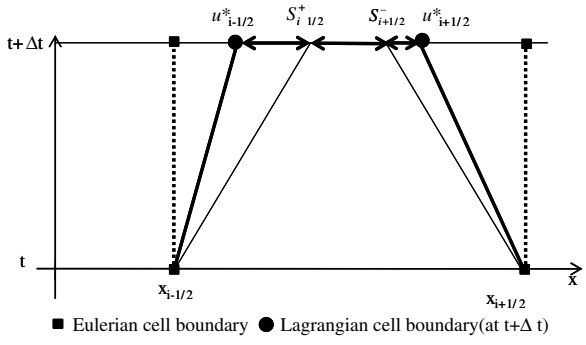

Fig. 4. Schematic view of the waves incoming a Lagrangian cell.

- $S^{+}_{i-1/2}$ represents a right-facing shock or rarefaction wave.
- $S^{-}_{i+1/2}$ represents a left-facing shock or rarefaction wave.

The volume of the cell at time t^{n+1} obeys the relation $\Delta x_i^{n+1} = \Delta x_i^n + \Delta t(u^*_{i+1/2} - u^*_{i-1/2})$.

This volume can be split into three sub-volumes, each of them containing the fluid in three different states: $L_1 = \Delta t(S^{+}_{i-1/2} - u^*_{i-1/2})$, $L_3 = \Delta t(u^*_{i+1/2} - S^{-}_{i+1:2})$; $L_2 = \Delta x_i^{n+1} - L_1 - L_3$.

Cell volume fractions can be defined: $\beta_j = \frac{L_j}{\Delta x_i^{n+1}}$, $j = 1, \ldots, 3$.

The Godunov projection then reads:

$$U_i^{n+1} = \sum_{j=1}^{3} \beta_j U_j^* \tag{2.1}$$

with $U_1^* = U^*_{R,i-1/2}, U_2^* = U_i^n, U_3^* = U^*_{L,i+1/2}$, where indexes L and R refer to left and right states in the Riemann problem. The Riemann problem solution allows the computation of the sub-volumes fractions β_j and of the state vectors $U_j^* = (\alpha_{1j}^*, \alpha_{1j}^*\rho_{1j}^*, \alpha_{2j}^*\rho_{2j}^*, \rho_j^* u_j^*, \rho_j^* E_j^*)^{\mathrm{T}}$ that contains the volume fraction variable. This provides a numerical scheme for the non-conservative volume fraction equation. The pressure is then computed with the mixture EOS (1.2). The results with this method are compared with the exact multiphase solution in Fig. 5 with the initial data of Fig. 3.

The agreement between the computed solution and the exact one is not perfect in particular regarding the volume fraction jump at shock front.

Let us mention that:

- The variables $\alpha_k\rho_k$ experience the same error in the jump as the mixture density.
- The error does not change when the exact Riemann solver is used. We have developed an extended version of Formula (2.1) when an exact solver is used instead of a 2-shocks approximate solver. It is more complex because expansion fans have to be integrated. No noticeable improvement of the solution was observed.
- The error remains the same under mesh refinement. An explanation of this observation is given in Section 5.1.

The convergence errors observed in Fig. 5 may be explained at least by two arguments:

- The first reason is that the volume fraction is not a conservative variable. Thus the average (2.1) for this variable has no physical sense.
- The second reason is that the sub-volumes fractions β_j have physical variations when the pressure in each sub-volume changes from the Riemann problem pressure p_j^* to the cell pressure computed with the mixture EOS (1.2) and cell averaged variables. A volume variation process is present in the cell, due to pressure relaxation, whose influence is not accounted for by (2.1).

In order to account for the sub-volumes fractions variations inside the computational cell a more sophisticated Lagrange method is derived to improve the accuracy.

3. A Lagrangian method based on internal energy equations

The reason why we use a Lagrangian scheme is due to the sound speed of the multiphase flows model. Acoustic waves propagates with the Wood [37] speed of sound whose non-monotonic behavior versus volume fraction is shown in Fig. 6 for the liquid water–air mixture.

Consider for example the advection of a liquid–gas interface, corresponding in this model to a volume fraction discontinuity. During numerical resolution, this discontinuity will become a mixture zone. In this zone, the sound speed has a non-monotonic behavior. It may result in the presence of two sonic points in the mixture zone even if the flow is subsonic in the two pure fluids. Capturing sonic points for this model poses difficulties as Riemann invariants cannot be integrated explicitly. Using an approximate Riemann solver where

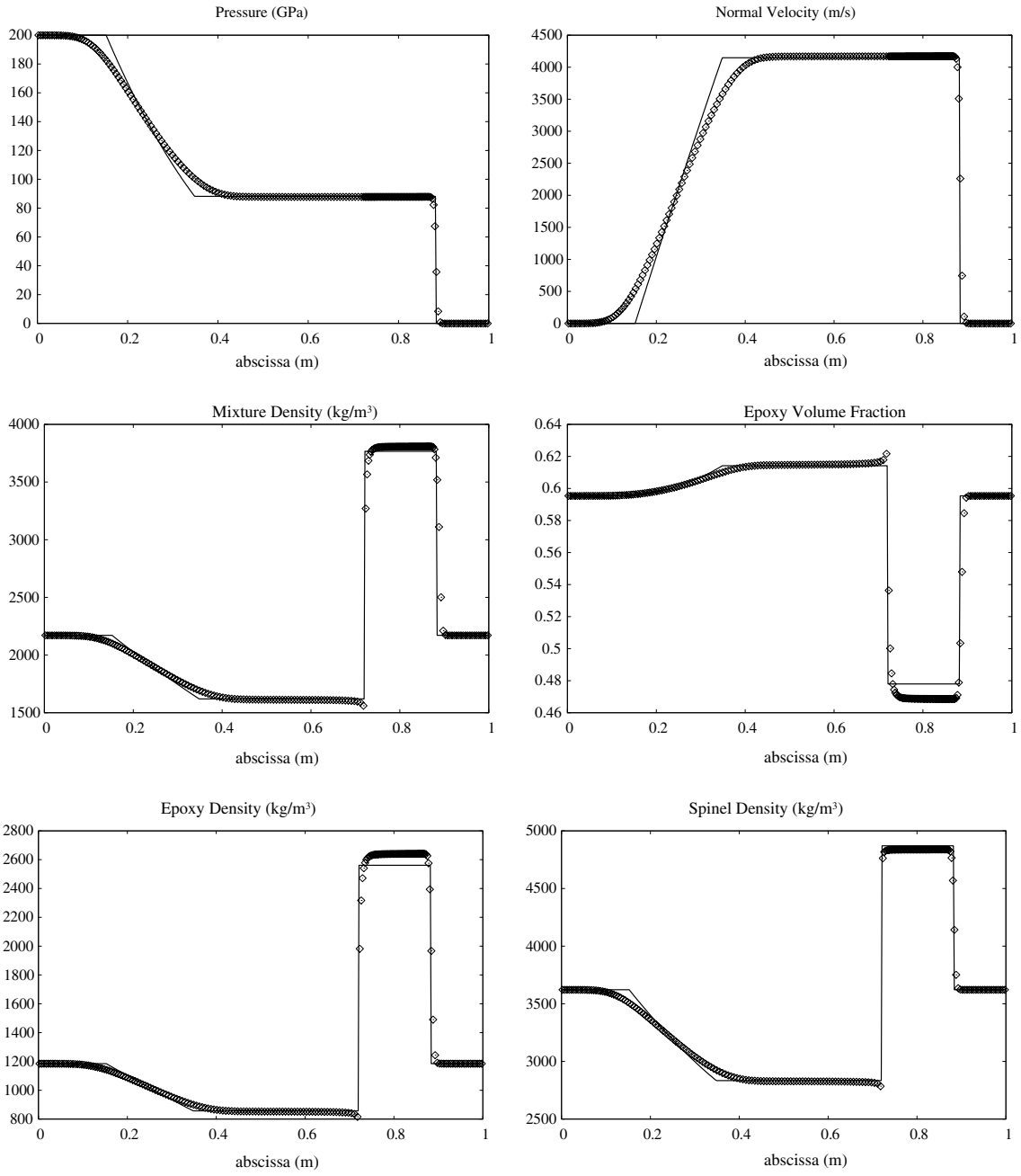

Fig. 5. Epoxy–spinel shock tube. Comparison of numerical results with a conventional Godunov type method (symbols) and the multiphase exact solution (solid). A 200 cells mesh is used. Convergence difficulties appear at the shock front.

the left and right facing waves are treated as discontinuities is possible. When embedded in an Eulerian method an error in the sampling of the solution for the fluxes computation will occur. This error will occur two times (for each sonic point) in the interface mixture zone for each time step. It finally result in computational difficulties and even failures. This difficulty is reported in the literature for barotropic flows with the same non-monotonic sound speed, used for example in cavitating flows [9,29,35]. These references report this problem in the simpler context of a conservative model.

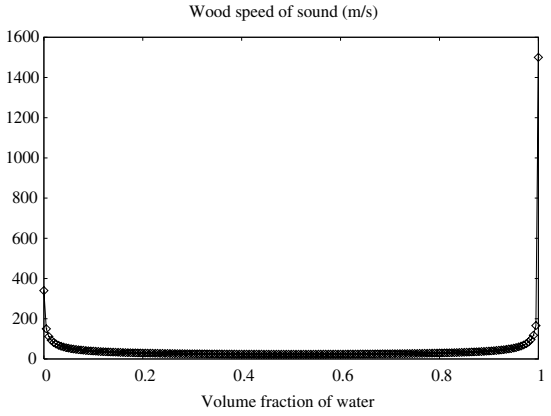

Fig. 6. Representation of the equilibrium mixture speed of sound ($\frac{1}{\rho c_w^2} = \frac{\alpha_1}{\rho_1 c_1^2} + \frac{\alpha_2}{\rho_2 c_2^2}$) for the liquid water–air mixture at atmospheric conditions.

There are at least two ways to circumvent this difficulty.

The first is to use a non-equilibrium model with relaxation. In the context of the present paper an appropriate model could be the seven equations model [5] that possesses frozen sound speed with monotonic behaviors. Accurate Eulerian methods are available for its resolution [2] that can be developed in unstructured grids [16].

The second option consists in using a Lagrange-projection method. The Lagrange step does not need the complete Riemann problem solution. In particular the expansion fan does not need resolution. The projection step can be done either with geometrical arguments in the context of the conventional Godunov method (2.1) or by a relaxation method, as developed in Saurel et al. [26]. In both cases, the presence of sonic points is transparent. However such method is difficult to extend in non-Cartesian grids. An extension by dimensional splitting on Cartesian grids will be presented. Obviously, this is a restriction. But most of the applications with interfaces, strong shocks and detonations can be done on Cartesian grids.

With the Lagrangian method the vector of conservative variables ($U = [\alpha_1\rho_1, \alpha_2\rho_2, \rho u, \rho E]^{\mathrm{T}}$) is updated unambiguously by the Godunov method:

$$(\overline{U}\Delta x)_i^{n+1} = (\overline{U}\Delta x)_i^n - \Delta t(F^*_{\mathrm{lag},i+1/2} - F^*_{\mathrm{lag},i-1/2}), \tag{3.1}$$

where $F_{\mathrm{lag}} = [0, 0, p, pu]^{\mathrm{T}}$ represents the Lagrangian flux and cell averages are defined by: $\overline{U}_i = \frac{1}{\Delta x_i}\int_{x_{i-1/2}}^{x_{i+1/2}} U\,\mathrm{d}x$. The superscript '$*$' denotes the solution of the Riemann problem. The evolution of the cell volume is given by: $\Delta x_i^{n+1} = \Delta x_i^n + \Delta t(u^*_{i+1/2} - u^*_{i-1/2})$.

From the conservative variables vector U mixture variables (ρ, u, e) can also be deduced.

The non-conservative volume fraction equation of system (1.0) and the saturation constraint ($\alpha_1 + \alpha_2 = 1$) can be replaced by non-conservative internal energy equations:

$$\frac{\mathrm{d}e_k}{\mathrm{d}t} + p\frac{\mathrm{d}v_k}{\mathrm{d}t} = 0, \quad k = 1, 2. \tag{3.2}$$

Time integration of these equations in cell i reads:

$$e_{i,k}^{n+1} - e_{i,k}^n + \tilde{p}_{i,k}(v_{i,k}^{n+1} - v_{i,k}^n) = 0 \quad \text{with } \tilde{p}_{i,k} = \frac{1}{(v_{i,k}^{n+1} - v_{i,k}^n)}\int_{t^n}^{t^{n+1}} p\frac{\mathrm{d}v_k}{\mathrm{d}t}\,\mathrm{d}t, \tag{3.3}$$

where the pressure averages $\tilde{p}_{i,k}$ have to be determined.

From system (3.1) it is possible to determine the evolution of the mixture internal energy:

$$e_i^{n+1} - e_i^n + \frac{(pu)^*_{i+1/2} - (pu)^*_{i-1/2} - \frac{u_i^{n+1}+u_i^n}{2}(p^*_{i+1/2} - p^*_{i-1/2})}{u^*_{i+1/2} - u^*_{i-1/2}}(v_i^{n+1} - v_i^n) = 0. \tag{3.4}$$

We now ask to the numerical approximation (3.3) to fulfil the same principles as the shock jump conditions (1.10) and (1.17):

- Equal pressure averages: $\tilde{p}_{i,1} = \tilde{p}_{i,2} = \tilde{p}_i$.
- Energy conservation. Summation of mass weighted energy Eqs. (3.3) yields:

$$(Y_{i,1}e_{i,1}^{n+1} + Y_{i,2}e_{i,2}^{n+1}) - (Y_{i,1}e_{i,1}^{n} + Y_{i,2}e_{i,2}^{n}) + \tilde{p}_i((Y_{i,1}v_{i,1}^{n+1} + Y_{i,2}v_{i,2}^{n+1}) - (Y_{i,1}v_{i,1}^{n} + Y_{i,2}v_{i,2}^{n})) = 0. \tag{3.5}$$

Identifying (3.4) and (3.5) the pressure average $\tilde{p}_i$ is deduced:

$$\tilde{p}_i = \frac{(pu)^*_{i+1/2} - (pu)^*_{i-1/2} - \frac{u_i^{n+1}+u_i^n}{2}(p^*_{i+1/2} - p^*_{i-1/2})}{u^*_{i+1/2} - u^*_{i-1/2}}. \tag{3.6}$$

Equations of the phase's internal energies (3.3) then read:

$$e_{i,k}^{n+1}(p_i^{n+1}, v_{i,k}^{n+1}) - e_{i,k}^{n}(p_i^{n}, v_{i,k}^{n}) + \tilde{p}_i(v_{i,k}^{n+1} - v_{i,k}^{n}) = 0, \quad k = 1, 2. \tag{3.7}$$

By inserting the phases EOS in this system the phases specific volumes express as:

$$v_{i,k}^{n+1} = v_{i,k}^{n+1}(p_i^{n+1}), \quad k = 1, 2. \tag{3.8}$$

The mass conservation constraint,

$$v_i^{n+1} = \sum_k Y_{i,k} v_{i,k}^{n+1}(p_i^{n+1}), \tag{3.9}$$

provides a nonlinear equation whose resolution yields the cell pressure p_i^{n+1}. In the context of SG EOS, the cell pressure reads:

$$p_i^{n+1} = -\sum_{k=1,2}\frac{A_{i,k}}{2} + \sum_{k=1,2}\frac{Y_{i,k}v_{i,k}^n B_{i,k}}{2v_i^{n+1}} + \sqrt{\left[\sum_{k=1,2}\frac{A_{i,k}}{2} - \sum_{k=1,2}\frac{Y_{i,k}v_{i,k}^n B_{i,k}}{2v_i^{n+1}}\right]^2 + \prod_{k=1,2}A_{i,k}\left(\sum_{k=1,2}\frac{Y_{i,k}v_{i,k}^n B_{i,k}}{v_i^{n+1}A_{i,k}} - 1\right)}. \tag{3.10}$$

With $A_{i,k} = (\gamma_k p_{\infty,k} + (\gamma_k - 1)\tilde{p}_i)$, $B_{i,k} = (p_i^n + \gamma_k p_{\infty,k} + (\gamma_k - 1)\tilde{p}_i)$, $k = 1, 2$.

For more general EOS a Newton–Raphson method is used. Once the cell pressure is determined, all remaining variables (volume fractions, specific volumes etc.) are readily obtained.

This method is tested under the same conditions as those of Fig. 5. The results are shown in Fig. 7.

In spite of the volume variations that are accounted for in the resolution of (3.9), convergence is not reached and no improvement is visible compared to the Godunov method. The main reason for the non-convergence of the two methods described in Sections 1 and 2 now appears as a consequence of the numerical diffusion of the shock front.

The shock front is solved as a succession of weak shocks whose thermodynamic path is different of the mixture Hugoniot curve defined by (1.10) and (1.17). It results in an incorrect partition of the internal energies or entropies of the phases. This last remark is the starting point of a deeper analysis and improved Lagrangian method. To restore the correct partition of the energies, artificial heat exchanges in the shock layer are introduced.

4. A Lagrangian method with artificial heat exchanges

4.1. Analysis of the numerical shock layer

Let us first recall some basic observation of numerical schemes in the context of single phase flows. To illustrate the presentation, let us consider the same shock tube test problem as previously where the spinel has been replaced by epoxy. It means that epoxy is present everywhere, at high pressure in the left chamber and at low pressure in the right chamber. The shock wave now evolves in a single phase fluid. It is interesting to compare

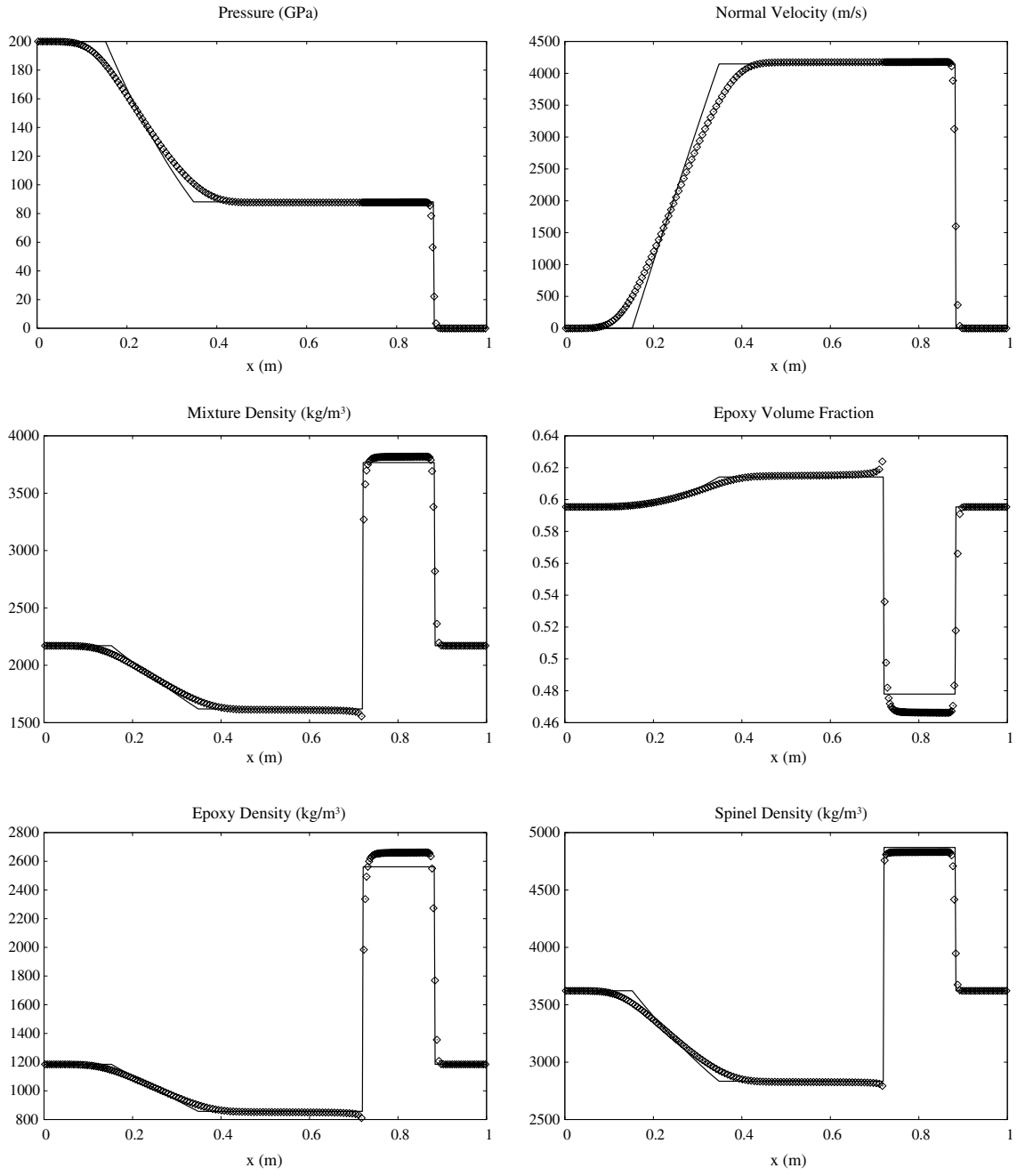

Fig. 7. Epoxy–spinel shock tube. Comparison of numerical results with the Lagrangian method based on internal energy equations (symbols) and the multiphase exact solution (solid). A 200 cells mesh is used. Convergence difficulties are again noticeable at the shock front.

the thermodynamic path followed by the fluid in the shock layer to the theoretical Hugoniot curve. Such comparison is shown in Fig. 8.

It appears clearly that the thermodynamic paths are very different. This is due to the succession of numerical weak shocks that propagate into the cell that do not impose the same thermodynamic transformation as a single strong shock [8]. The successive cell averages produce also transformations in disagreement with the single shock Hugoniot.

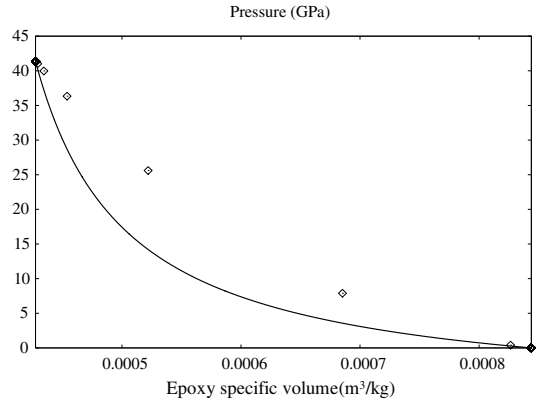

Fig. 8. Comparison of the numerical Hugoniot curve (symbols) and the theoretical one (lines) in the numerical diffusion zone for single phase flows. The two thermodynamic paths are different but the end states are the same.

However, this numerical phenomenon has no consequence on the computation of the shocked state for single phase flows. As shown in Fig. 8, the end of the shock layer merges with the theoretical Hugoniot state. This is a consequence of conservation properties of the Euler equations.

When dealing with multiphase mixtures, the same deviation from the theoretical Hugoniot appears and has more serious consequences as observed previously in Sections 1 and 2. The reason is that for each weak shock that enter the cell, the equation of state changes. Indeed, for multiphase mixtures, there is an extra degree of freedom characterized by the volume fraction. At a given point of the numerical shock, as shown in Fig. 8, there is no hope that this point belongs to the theoretical mixture Hugoniot curve. It follows that the corresponding volume fraction is in error. Consequently, the mixture EOS (1.2) is in error too. These errors cumulate along the shock layer and contrarily to single phase flows, the end state does not belong to the mixture Hugoniot.

To illustrate this difficulty, the numerical phases and mixture Hugoniot curves are compared to the theoretical ones in Fig. 9.

Shock tracking is an option to cure such difficulty [11,17,19]. Another option is to correct partition of the energies in the shock layer by introducing artificial heat transfers.

4.2. Artificial heat exchanges

In the presence of heat transfers, the single velocity and single pressure two-phase flow model reads [13]:

$$
\begin{aligned}
&\frac{\partial \alpha_1}{\partial t} + u\frac{\partial \alpha_1}{\partial x} = \frac{\rho_2 c_2^2 - \rho_1 c_1^2}{\frac{\rho_1 c_1^2}{\alpha_1} + \frac{\rho_2 c_2^2}{\alpha_2}}\frac{\partial u}{\partial x} + \frac{\alpha_1\alpha_2}{\alpha_2\rho_1 c_1^2 + \alpha_1\rho_2 c_2^2}\left(\frac{\Gamma_1}{\alpha_1} + \frac{\Gamma_2}{\alpha_2}\right)H(T_2 - T_1),\\
&\frac{\partial \alpha_1\rho_1}{\partial t} + \frac{\partial \alpha_1\rho_1 u}{\partial x} = 0,\\
&\frac{\partial \alpha_2\rho_2}{\partial t} + \frac{\partial \alpha_2\rho_2 u}{\partial x} = 0,\\
&\frac{\partial \rho u}{\partial t} + \frac{\partial (\rho u^2 + p)}{\partial x} = 0,\\
&\frac{\partial \rho E}{\partial t} + \frac{\partial (\rho E + p)u}{\partial x} = 0,
\end{aligned}
\tag{4.1}
$$

where $\Gamma_k = (v_k\frac{\partial p_k}{\partial e_k})_{v_k}$ represents the Grüneisen coefficient of phase k. Heat exchange is modeled with a simple exchange coefficient H that accounts for the thermal conductivities and exchange surface. The internal energy equations now read:

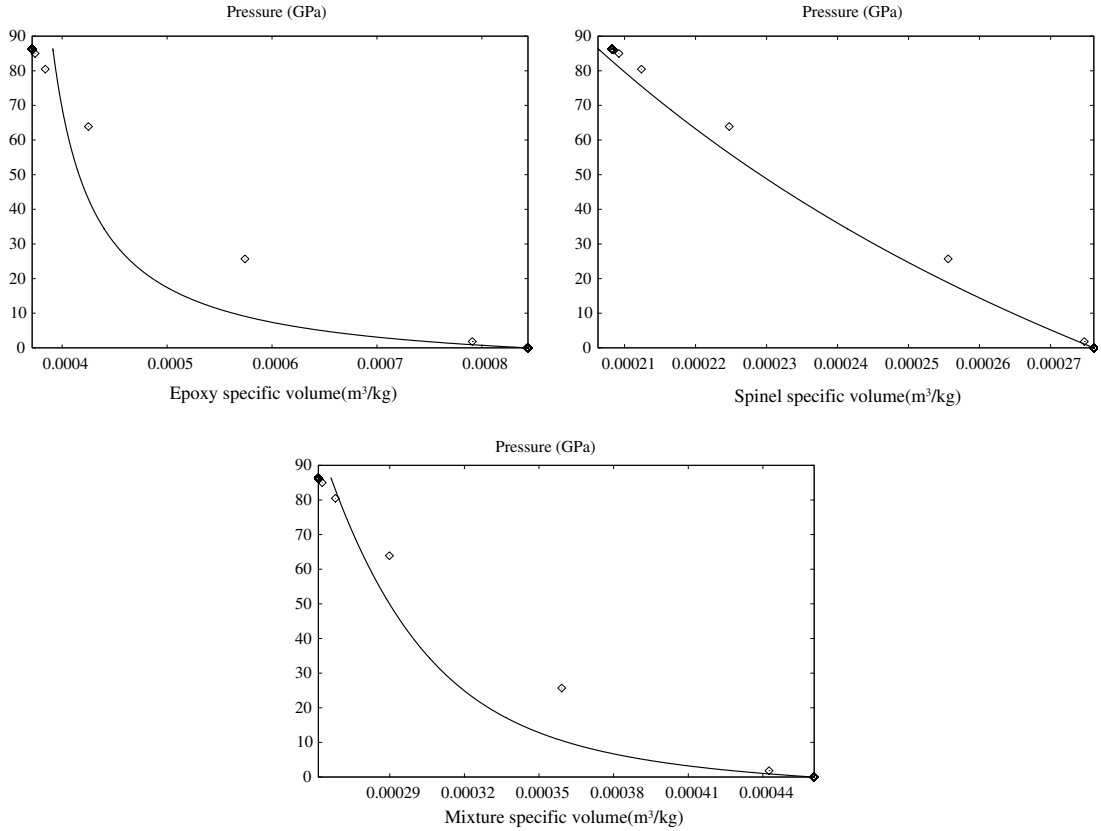

Fig. 9. Comparison of numerical Hugoniot curves (symbols) and theoretical ones (lines) in the numerical shock layer. The same conditions as those of Fig. 7 are used with the same numerical scheme. The final state is not correctly computed.

$$\begin{aligned}\frac{de_1}{dt}+p\frac{dv_1}{dt}&=\frac{H}{Y_1\rho}(T_2-T_1),\\ \frac{de_2}{dt}+p\frac{dv_2}{dt}&=-\frac{H}{Y_2\rho}(T_2-T_1).\end{aligned}\tag{4.2}$$

Obviously this modeling is in agreement with the entropy inequality:

$$\frac{ds}{dt}=\frac{d(Y_1s_1+Y_2s_2)}{dt}=\frac{H}{\rho T_1T_2}(T_2-T_1)^2\geqslant 0.$$

In order to express heat exchanges under differential form an asymptotic analysis is achieved. This differential form is needed in order that heat exchanges be present in the shock layer only. We assume stiff thermal relaxation: $H=\frac{H^0}{\varepsilon}$ where $\varepsilon\to 0^+$. Stiffness of thermal relaxation remains however slow compared to mechanical relaxation [13]. Each flow variable f is expressed by the asymptotic expansion: $f=f^0+\varepsilon f^1$ where f^0 represents the equilibrium state and f^1 a fluctuation.

At order $\frac{1}{\varepsilon}$ the energy equations imply: $T_2^0=T_1^0$.

At zero order they become:

$$\begin{aligned}\frac{de_1^0}{dt}+p^0\frac{dv_1^0}{dt}&=\frac{H^0}{Y_1^0\rho^0}(T_2^1-T_1^1),\\ \frac{de_2^0}{dt}+p^0\frac{dv_2^0}{dt}&=-\frac{H^0}{Y_2^0\rho^0}(T_2^1-T_1^1).\end{aligned}$$

In terms of temperatures, they become:

$$\frac{\mathrm{d}T_1^0}{\mathrm{d}t} = \frac{\Gamma_1^0 T_1^0}{\alpha_1^0}\left\{\left(\frac{1}{\rho_1^0\Gamma_1^0 c_{v,1}^0 T_1^0} - \frac{\rho^0 {c_w^0}^2}{\rho_1^0 {c_1^0}^2 \rho_2^0 {c_2^0}^2}\frac{\Gamma_1^0\Gamma_2^0}{\Gamma^0}\right)H^0(T_2^1 - T_1^1) - \left(\frac{\rho^0 {c_w^0}^2 \alpha_1^0\alpha_2^0(\rho_2^0 {c_2^0}^2 - \rho_1^0 {c_1^0}^2)}{\rho_1^0 {c_1^0}^2 \rho_2^0 {c_2^0}^2} + \alpha_1^0\right)\frac{\partial u^0}{\partial x}\right\},$$

$$\frac{\mathrm{d}T_2^0}{\mathrm{d}t} = -\frac{\Gamma_2^0 T_2^0}{\alpha_2^0}\left\{\left(\frac{1}{\rho_2^0\Gamma_2^0 c_{v,2}^0 T_2^0} - \frac{\rho^0 {c_w^0}^2}{\rho_1^0 {c_1^0}^2 \rho_2^0 {c_2^0}^2}\frac{\Gamma_1^0\Gamma_2^0}{\Gamma^0}\right)H^0(T_2^1 - T_1^1) - \left(\frac{\rho^0 {c_w^0}^2 \alpha_1^0\alpha_2^0(\rho_2^0 {c_2^0}^2 - \rho_1^0 {c_1^0}^2)}{\rho_1^0 {c_1^0}^2 \rho_2^0 {c_2^0}^2} - \alpha_2^0\right)\frac{\partial u^0}{\partial x}\right\}.$$

The 'heat exchange' thus expresses:

$$(T_2^1 - T_1^1) = \frac{\alpha_1^0\alpha_2^0}{H^0}\left(\frac{\rho^0 {c_w^0}^2\left(\rho_2^0 {c_2^0}^2 - \rho_1^0 {c_1^0}^2\right)\frac{\Gamma_1^0\Gamma_2^0}{\Gamma^0} - \rho_1^0 {c_1^0}^2 \rho_2^0 {c_2^0}^2(\Gamma_2^0 - \Gamma_1^0)}{\frac{{c_1^0}^2 {c_2^0}^2}{T_1^0}\left(\frac{\alpha_2^0\rho_2^0}{c_{v,1}^0} + \frac{\alpha_1^0\rho_1^0}{c_{v,2}^0}\right) - \rho^0 {c_w^0}^2\left(\frac{\Gamma_1^0\Gamma_2^0}{\Gamma^0}\right)^2}\right)\frac{\partial u^0}{\partial x}.$$

This asymptotic form of the heat transfer is now inserted in the non-equilibrium flow model (4.1) and (4.2) where superscript '0' are omitted for the sake of clarity:

$$\begin{aligned}
&\frac{\partial \alpha_1\rho_1}{\partial t} + \frac{\partial \alpha_1\rho_1 u}{\partial x} = 0,\\
&\frac{\partial \alpha_2\rho_2}{\partial t} + \frac{\partial \alpha_2\rho_2 u}{\partial x} = 0,\\
&\frac{\partial \rho u}{\partial t} + \frac{\partial(\rho u^2 + p)}{\partial x} = 0,\\
&\frac{\mathrm{d}e_1}{\mathrm{d}t} + p\frac{\mathrm{d}v_1}{\mathrm{d}t} = \frac{1}{\rho Y_1}\left\{\alpha_1\alpha_2\left(\frac{\rho c_w^2\left(\rho_2 c_2^2 - \rho_1 c_1^2\right)\frac{\Gamma_1\Gamma_2}{\Gamma} - \rho_1 c_1^2\rho_2 c_2^2(\Gamma_2 - \Gamma_1)}{\frac{c_1^2 c_2^2}{T_1}\left(\frac{\alpha_2\rho_2}{c_{v,1}} + \frac{\alpha_1\rho_1}{c_{v,2}}\right) - \rho c_w^2\left(\frac{\Gamma_1\Gamma_2}{\Gamma}\right)^2}\right)\right\}\frac{\partial u}{\partial x},\\
&\frac{\mathrm{d}e_2}{\mathrm{d}t} + p\frac{\mathrm{d}v_2}{\mathrm{d}t} = -\frac{1}{\rho Y_2}\left\{\alpha_1\alpha_2\left(\frac{\rho c_w^2(\rho_2 c_2^2 - \rho_1 c_1^2)\frac{\Gamma_1\Gamma_2}{\Gamma} - \rho_1 c_1^2\rho_2 c_2^2(\Gamma_2 - \Gamma_1)}{\frac{c_1^2 c_2^2}{T_1}\left(\frac{\alpha_2\rho_2}{c_{v,1}} + \frac{\alpha_1\rho_1}{c_{v,2}}\right) - \rho c_w^2\left(\frac{\Gamma_1\Gamma_2}{\Gamma}\right)^2}\right)\right\}\frac{\partial u}{\partial x}.
\end{aligned} \tag{4.3}$$

This limit model agrees with the entropy inequality:

$$\frac{\mathrm{d}s}{\mathrm{d}t} = \frac{\mathrm{d}(Y_1 s_1 + Y_2 s_2)}{\mathrm{d}t} = \frac{1}{HT_1T_2\rho}\left(\alpha_1\alpha_2\left(\frac{\rho c_w^2(\rho_2 c_2^2 - \rho_1 c_1^2)\frac{\Gamma_1\Gamma_2}{\Gamma} - \rho_1 c_1^2\rho_2 c_2^2(\Gamma_2 - \Gamma_1)}{\frac{c_1^2 c_2^2}{T_1}\left(\frac{\alpha_2\rho_2}{c_{v,1}} + \frac{\alpha_1\rho_1}{c_{v,2}}\right) - \rho c_w^2\left(\frac{\Gamma_1\Gamma_2}{\Gamma}\right)^2}\right)\frac{\partial u}{\partial x}\right)^2 \geqslant 0. \tag{4.4}$$

This model will be used inside the shock layer only. As the shock width is small, thermal equilibrium is not reached even if thermal relaxation is stiff.

Model (4.3) is obviously non-conservative and the integration of the term in factor of the velocity divergence is an issue. Moreover, our aim is not to deal with physical heat exchanges, but with artificial ones inside the shock layer. To build a reliable approximation method, the information coming from the physics are used. We now introduce some simplifications. Inside the shock layer, all flow variables that appear in factor of the velocity divergence are function of the shock speed or any other flow variable. We decide to express these flow variables as function of the mixture specific volume. Expressing the mixture mass conservation equation under the form:

$$\frac{\mathrm{d}v}{\mathrm{d}t} - v\frac{\partial u}{\partial x} = 0.$$

The internal energy equations (4.3) thus read:

$$\frac{de_1}{dt} + p\frac{dv_1}{dt} = \frac{1}{Y_1} v(v) \frac{dv}{dt},$$
$$\frac{de_2}{dt} + p\frac{dv_2}{dt} = -\frac{1}{Y_2} v(v) \frac{dv}{dt}.$$

These equations can be written under a more practical form:

$$\begin{aligned} &\frac{de_1}{dt} + p\frac{dv_1}{dt} = \frac{1}{Y_1} \frac{d\mu(v)v}{dt}, \\ &\frac{de_2}{dt} + p\frac{dv_2}{dt} = -\frac{1}{Y_2} \frac{d\mu(v)v}{dt}, \end{aligned} \tag{4.5}$$

where functions v and μ are linked by the relation: $v(v) = v\mu'(v) + \mu(v)$. Presentation of the energy equations under formulation (4.5) facilitates integration and provides, as will be shown later, mesh independent results.

Integration of Eqs. (4.5) during a time step yields the following numerical scheme:

$$\begin{aligned} &e_{i,1}^{n+1} - e_{i,1}^{n} + \tilde{p}_i(v_{i,1}^{n+1} - v_{i,1}^{n}) = \eta\left(\frac{\partial u}{\partial x}\right) \frac{1}{Y_{i,1}} [\mu(v^{n+1})v^{n+1} - \mu(v^n)v^n] = Q_{i,1}, \\ &e_{i,2}^{n+1} - e_{i,2}^{n} + \tilde{p}_i(v_{i,2}^{n+1} - v_{i,2}^{n}) = -\eta\left(\frac{\partial u}{\partial x}\right) \frac{1}{Y_{i,2}} [\mu(v^{n+1})v^{n+1} - \mu(v^n)v^n] = Q_{i,2}, \end{aligned} \tag{4.6}$$

where

$$\eta\left(\tfrac{\partial u}{\partial x}\right) = \begin{cases} 1 & \text{if } \tfrac{\partial u}{\partial x} < 0, \\ 0 & \text{otherwise.} \end{cases}$$

The function η guarantees that heat exchanges will be used in the shock layer only.

The closure of this method necessitates the determination of the heat exchange function μ. This issue is addressed in the next paragraph. Once this function is determined, the numerical scheme corresponds to:

- Relations (3.1) for the conservative variables,
- Relation (3.6) for the pressure average estimate,
- Relations (4.6) for the update of the internal energies (they replace Relations (3.7) of the preceding algorithm).
- Relation (3.10) is replaced by:

$$p_i^{n+1} = -\sum_{k=1,2} \frac{A_{i,k}}{2} + \sum_{k=1,2} \frac{Y_{i,k}[v_{i,k}^n B_{i,k} + (\gamma_k - 1)Q_{i,k}]}{2v_i^{n+1}} + \sqrt{\left[\sum_{k=1,2} \frac{A_{i,k}}{2} - \sum_{k=1,2} \frac{Y_{i,k}\left[v_{i,k}^n B_{i,k} + (\gamma_k - 1)Q_{i,k}\right]}{2v_i^{n+1}}\right]^2 + \prod_{k=1,2} A_{i,k} \left(\sum_{k=1,2} \frac{Y_{i,k}[v_{i,k}^n B_{i,k} + (\gamma_k - 1)Q_{i,k}]}{v_i^{n+1} A_{i,k}} - 1\right)}. \tag{4.7}$$

With $A_{i,k} = (\gamma_k p_{\infty,k} + (\gamma_k - 1)\tilde{p}_i), B_{i,k} = (p_i^n + \gamma_k p_{\infty,k} + (\gamma_k - 1)\tilde{p}_i),\ k = 1, 2.$

This method is tested on the same shock tube test problem as those of Fig. 7. Corresponding results are shown in Fig. 10.

Artificial heat exchanges considerably improve the results. The method is mesh independent as shown in Fig. 11.

4.3. Determination of the heat exchange function μ

For a given two-phase mixture (epoxy–spinel for example), in a given initial state $(v_0, u_0, p_0, Y_{10}, \alpha_{10})$, function μ is constructed step by step by piecewise linear approximations. The construction method is based on the

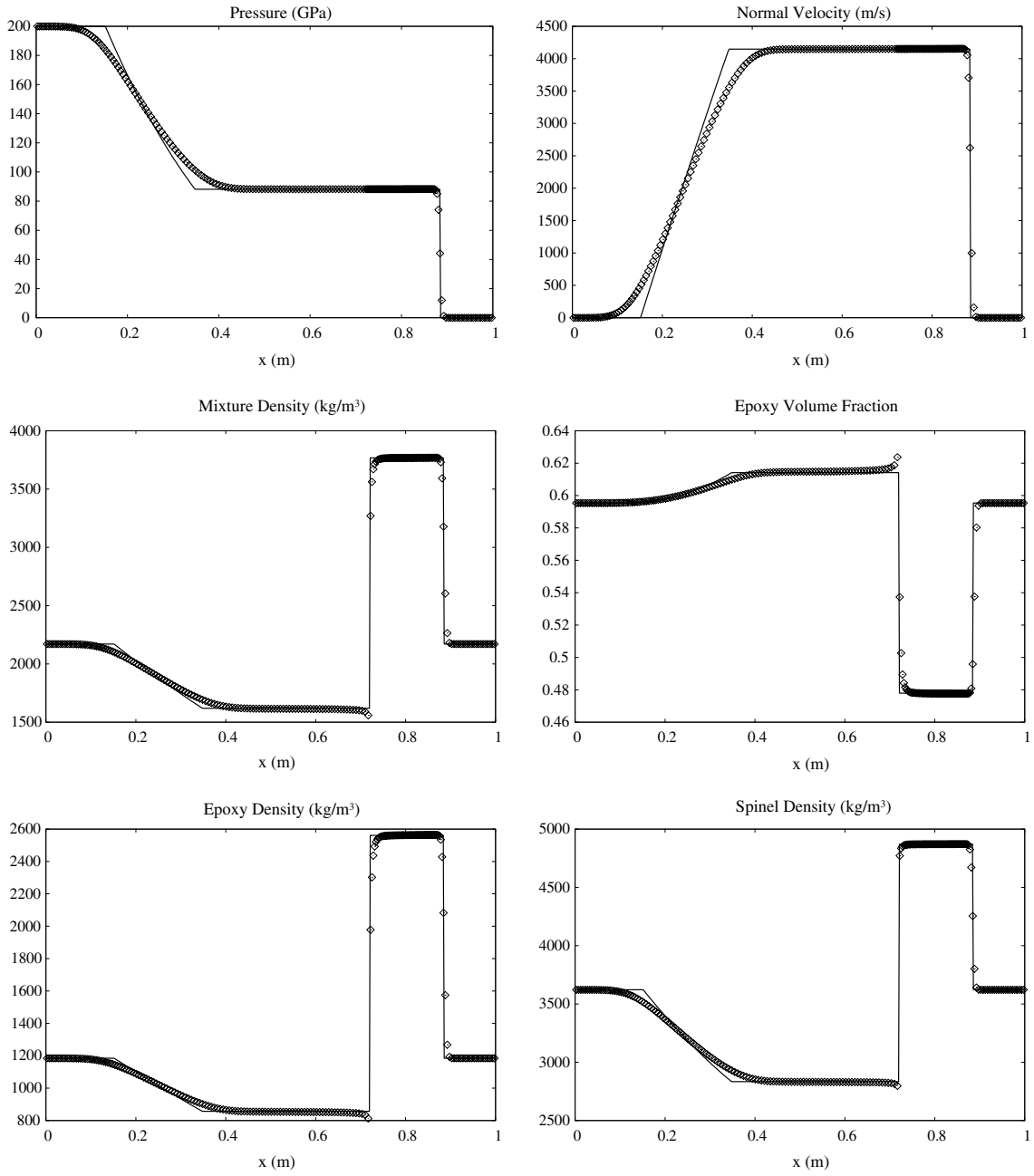

Fig. 10. Epoxy–spinel shock tube. Comparison of numerical results with the Lagrangian method including artificial heat exchanges in the shock layer (symbols) and the multiphase exact solution (solid). A 200 cells mesh is used. Accuracy of the results is considerably improved.

comparison of computed results with the preceding numerical scheme and exact solution obtained for shock relations or exact Riemann problem solution detailed in Section 1.1.

For weak shocks no correction is necessary. Thus, in the range $[v_0; v_1]$, $\mu(v)$ is taken equal to zero. v_0 represents the specific volume at standard state and v_1 the limit of specific volume where accurate results are obtained without heat exchanges correction.

When the shock becomes stronger, up to a specific volume v_2, μ is approximated by a linear function $\mu_1(v) = a_1(v - v_1)$. The slope a_1 of the function is determined in order that the agreement between computed and exact results be perfect in the shocked specific volume range $[v_1; v_2]$.

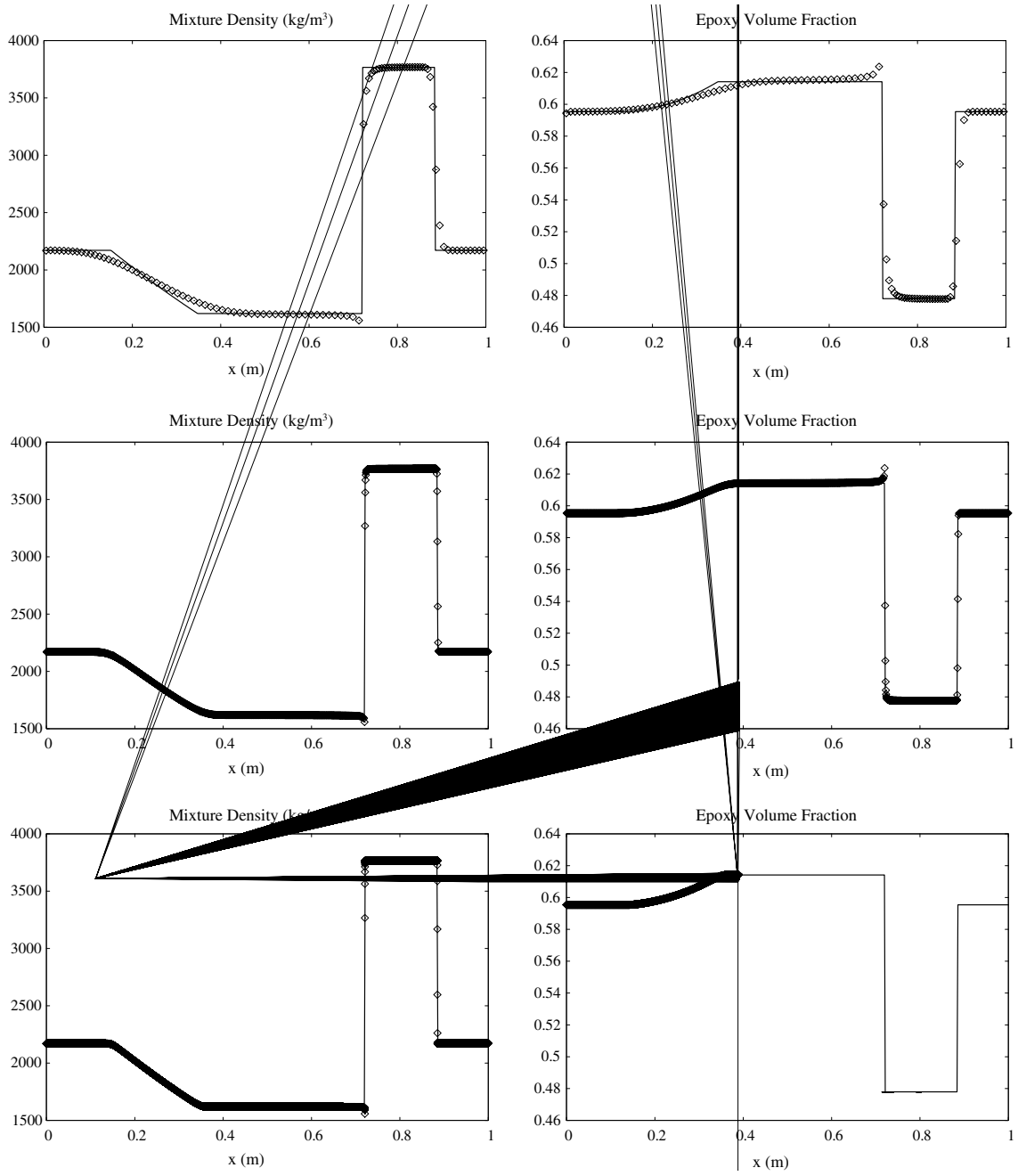

Fig. 11. Epoxy–spinel shock tube. Comparison of numerical results with the Lagrangian method including artificial heat exchanges in the shock layer (symbols) and the multiphase exact solution (solid). From top to bottom: 100, 1000 and 10,000 cells are used. The method is mesh independent.

Then up to a new value of the specific volume v_3, μ is approximated by a new linear function $\mu_2(v) = a_2(v - v_2) + \mu_1(v_2)$. The new slope a_2 is determined in order that the agreement between numerical and exact solutions be perfect in the shocked specific volume range $[v_2; v_3]$.

This procedure is repeated about 10 times in the specific volume range under interest $[v_0; v_*]$ where v_* represents the maximum shocked specific volume in the pressure range under interest. For example, pressure range of the order of 1–1,000,000 atm is considered here.

The piecewise linear function μ is then fitted by a reduced function, as shown in Fig. 12.

The fitted function $\bar{\mu}$ is directly used in the numerical scheme based on (4.6). Excellent agreement with the exact solution is obtained. There are however some restrictions:

- The function $\bar{\mu}$ is valid only for shock waves propagating in a mixture of initial state $(v_0, u_0, p_0, Y_{10}, \alpha_{10})$.
- It is valid for the numerical scheme used for the calibration of the function $\bar{\mu}$. This is not surprising as any numerical scheme has its own numerical diffusion. For example, if the order of accuracy is increased, the function $\bar{\mu}$ has to be re-determined by the procedure described previously.

In order to illustrate the validity of the method for shocks of arbitrary strength in a given initial two-phase mixture, various shock tube tests are done. The function $\bar{\mu}$ of Fig. 12 is implemented and tested for different shock intensities propagating into the epoxy–spinel mixture of previous sections. Results are shown in Fig. 13. For each shock intensity, they show a perfect agreement.

5. Eulerian scheme

The Eulerian scheme is derived from the preceding Lagrangian scheme by projecting the solution on the Eulerian grid. However, the presence of a non-conservative variable prevents the use of a conventional projection method (Godunov projection for example). A specific relaxation-projection method was introduced in Saurel et al. [26] in the context of the Euler equations. This method is based on a multiphase description of the flow inside a computational cell. Its framework is thus extended easily to the present context of multiphase mixtures.

5.1. Relaxation system

The propagation of the various Lagrangian cell boundaries in the Eulerian cell delimitate a maximum of three sub-volumes in the computational cell, as shown in Fig. 4. These sub-volumes are in fact segments whose lengths are directly obtained from the Lagrangian cells boundaries velocities:

$$L_1 = \max(0, u^*_{i-1/2})\Delta t; \quad L_3 = -\min(0, u^*_{i+1/2})\Delta t; \quad L_2 = \Delta x_i - L_1 - L_3.$$

Normalized length correspond to sub-volumes fractions $\beta_j = \frac{L_j}{\Delta x_i}$, $j = 1, \ldots, 3$.

In the present multiphase flows context, each sub-volume contains now several phases k with volume fractions α_k.

At the end of the Lagrange step, each Lagrangian cell contains a state in disequilibrium with its neighboring cells states. It means that the Eulerian cell also contains three sub-volumes with three non-equilibrium states. In particular, three different velocities and pressures are present in the cell. Determination of the average state in the Eulerian cell consists in determining the equilibrium state that results of the acoustic interactions with the various sub-volumes and states. This equilibrium state is only a mechanical equilibrium one: all pressures and velocities must relax to an equilibrium pressure and velocity. The temperatures must remain in non-equilibrium. Following Saurel et al. [26] the multiphase extension of the relaxation system that drives the various sub-cell states to mechanical equilibrium reads:

$$\begin{aligned}
&\frac{\partial \alpha_{jk}\beta_j}{\partial \tau} = \frac{\delta}{Z_{jk}}(p_j - p_I),\\
&\frac{\partial \alpha_{jk}\beta_j\rho_{jk}}{\partial \tau} = 0,\\
&\frac{\partial \alpha_{jk}\beta_j\rho_{jk}u_j}{\partial \tau} = \delta Z_{jk}(u_I - u_j),
\end{aligned} \tag{5.1}$$

$$\frac{\partial \alpha_{jk}\beta_j\rho_{jk}E_{jk}}{\partial \tau} = \delta\left(u_I Z_{jk}(u_I - u_j) - \frac{p_I}{Z_j}(p_j - p_I)\right) \quad \text{with } u_I = \frac{\sum_{jk} Z_{jk}u_j}{\sum_{jk} Z_{jk}} \text{ and } p_I = \frac{\sum_{jk}\frac{p_j}{Z_{jk}}}{\sum_{jk}\frac{1}{Z_{jk}}}, \tag{5.2}$$

where α_{jk} represents the volume fraction of phase k in the sub-volume j, with $j = 1,2,3$ and $k = 1,2,\ldots,K$. K is the total number of phases. The acoustic impedance of phase k is defined by: $Z_k = \rho_k c_k$.

The solution of this system when $\tau \to +\infty$ provides the relaxed mechanical equilibrium state. It can be shown easily that system (5.1) guarantees conservation properties of the mixture and entropy production.

As only the relaxed asymptotic state is required, a time accurate integration of (4.1) is unnecessary. Approximate integration of the energy equations reads:

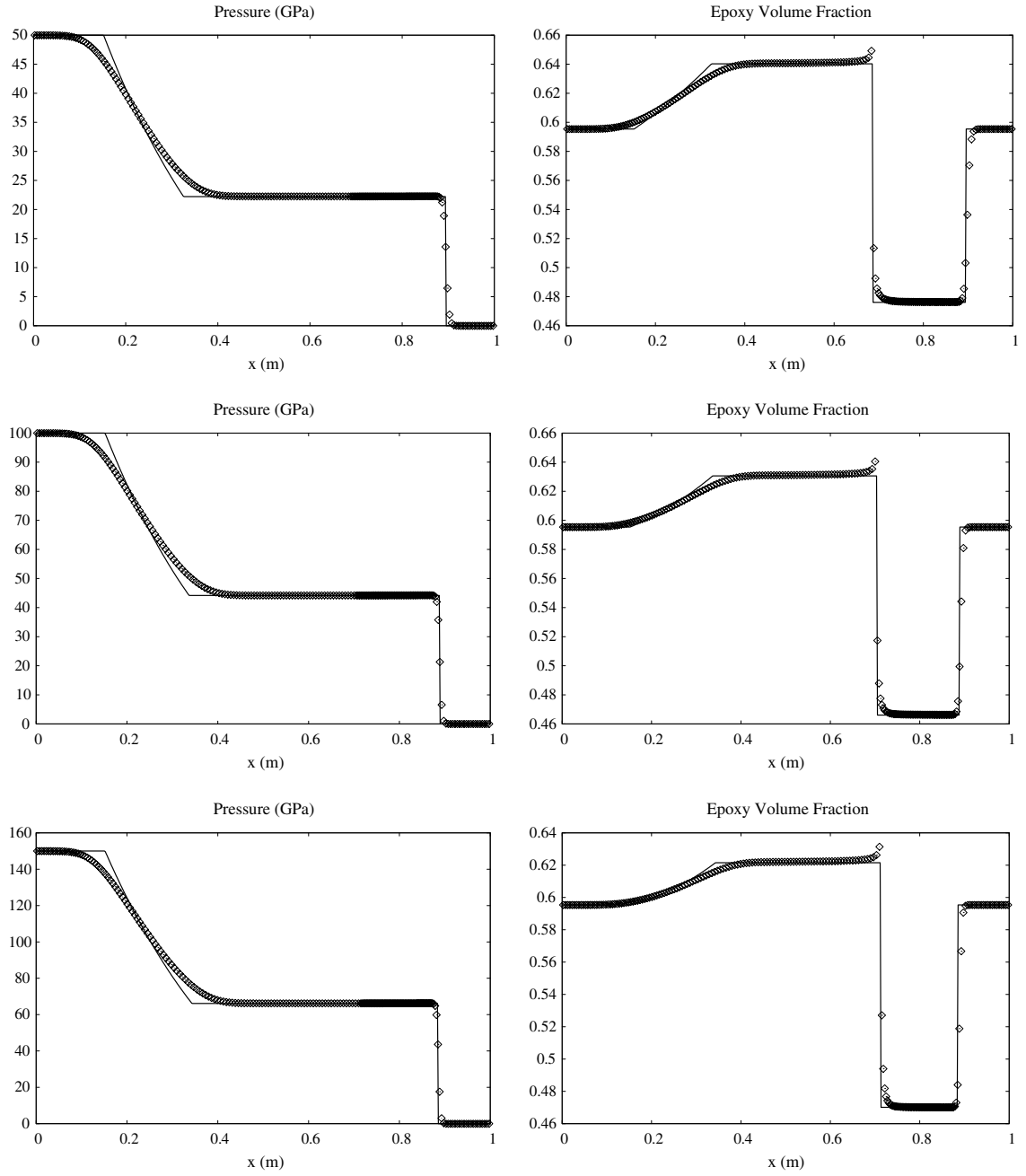

Fig. 13. Accuracy of the heat exchange function $\bar{\mu}$ for different shock intensities. From top to bottom, pressure in the high pressure chamber is set to 50, 100 and 150 GPa. For each shock intensity, results are in perfect agreement.

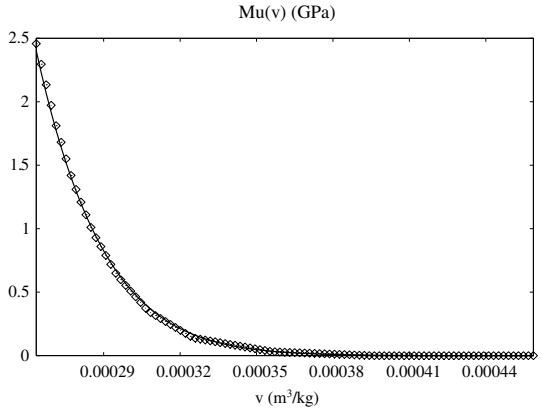

Fig. 12. Values of the approximate piecewise linear function of μ (symbols) and fitting curve ($\bar{\mu}(v) = \exp[-8.34 \times 10^7 \times v^2 + 5.83^3 \times v + 25.9]$) in the specific volume range (2.65×10^{-4}–4.61×10^{-4} m^3/kg) corresponding to piston velocity range of 0–4200 m/s and pressure range of 1–880,000 atm.

$$e^*_{jk} - e^0_{jk} + \hat{p}_{Ijk}(v^*_{jk} - v^0_{jk}) = q_{jk} \tag{5.3}$$

with $q_{jk} = \frac{1}{2}(u^* - u^0_j)(2\hat{u}_{Ijk} - (u^* + u^0_j))$.The choice of averaged interfacial variables is linked to the two following constraints:

- energy conservation,
- entropy inequality.

In the single phase flows context examined in Saurel et al. [26] it was shown that $\hat{u}_{Ij} = u^*$ and $\hat{p}_{Ij} = p^*$ were simple estimates to satisfy these constraints and accurate enough to build an algorithm for single phase flows. In the multiphase flow context, these estimates are still admissible. Energy conservation is obviously fulfilled and approximate integration of the entropy equations reads:

$$T^0_{jk}(s^*_{jk} - s^0_{jk}) = \frac{1}{2}\frac{\gamma_{jk}}{\Gamma_{jk}}\frac{(u^* - u^0_j)^2 {Z^0_{jk}}^2 + (p^* - p^0_j)^2}{\left({Z^*_{jk}}^2 + {Z^0_{jk}}^2\left(\frac{\gamma_{jk}}{\Gamma_{jk}} - 1\right)\right)}. \tag{5.4}$$

More sophisticated estimates have been found under preceding constraints and tested numerically. Few differences were observed. Thus we retain in the present study:

$$\hat{u}_{Ij} = u^* \quad \text{and} \quad \hat{p}_{Ij} = p^*. \tag{5.5}$$

5.2. Algorithm

Let us denote with superscript '0' the variables in the Lagrangian sub-volumes. Superscript '$*$' will denote the relaxed state, or cell averaged variables.

The mass conservation of the mixture implies:

$$\rho^* = \sum_{jk} \beta^*_j \alpha^*_{jk} \rho^*_{jk} = \sum_{jk} \beta^0_j \alpha^0_{jk} \rho^0_{jk} = \rho^0 = \rho, \tag{5.6}$$

and the mass conservation of the phases read:

$$(\alpha\rho)^*_k = \sum_j \beta^*_j \alpha^*_{jk} \rho^*_{jk} = \sum_j \beta^0_j \alpha^0_{jk} \rho^0_{jk} = (\alpha\rho)^0_k = (\alpha\rho)_k. \tag{5.7}$$

Conservation of the mixture momentum reads:

$$\sum_{jk} \beta_j^* \alpha_{jk}^* \rho_{jk}^* u_j^* = \sum_{jk} \beta_j^0 \alpha_{jk}^0 \rho_{jk}^0 u_j^0. \tag{5.8}$$

The relaxed state is characterized by a unique velocity $u_j^* = u^*$. Eq. (5.9) thus provides the relaxed velocity:

$$u^* = \frac{\sum_{jk} \beta_j^0 \alpha_{jk}^0 \rho_{jk}^0 u_j^0}{\sum_{jk} \beta_j^0 \alpha_{jk}^0 \rho_{jk}^0}. \tag{5.9}$$

The determination of the relaxed pressure requires the use of the phases EOS: $e_k = e_k(v_k, p_k)$.

For a given cell, p^* and the $v_{jk}^* (j = 1, 2, 3;\ k = 1, \ldots, K)$ form a set of $3K + 1$ unknowns.

Relation (5.4) with (5.6) provides $3K$ equations that may be written as:

$$e_{jk}^*(v_{jk}^*, p*) - e_{jk}^0 + p^*(v_{jk}^* - v_{jk}^0) = \frac{1}{2}(u^* - u_j^0)^2. \tag{5.10}$$

The last equation to close the system is obtained by the saturation constraint ($\sum_{jk} \beta_j \alpha_{jk} = 1$) under the form:

$$\sum_{jk} m_{jk} v_{jk}(p^*) - 1 = 0, \tag{5.11}$$

where $m_{jk} = \beta_j \alpha_{jk} \rho_{jk}$ denotes the mass in each sub-volume, which is constant during the relaxation process.

System (5.10) completed by (5.11) forms a non-linear systems solved by a Newton–Raphson method. Actually, the iterative process only depends on the pressure p^* and this method is not very expensive in computational time.

However, it is possible to replace this iterative procedure by a direct one when the computation does not contain strong pressure gradient. Following again [26], when $\mathrm{Max}_j(\frac{p_j - p_1}{p_1}) < \varepsilon$ (typically $\varepsilon = 0.01$) the mixture EOS (1.2) can be used under the form:

$$p^* = \frac{\sum_{jk} \beta_j^0 \alpha_{jk}^0 \rho_{jk}^0 \left(e_{jk}^0 + \frac{1}{2} u_j^0\right) - \frac{1}{2} \rho u^{*2} - \sum_k \left(\frac{\gamma_k p_{\infty k}}{\gamma_k - 1} \sum_j \beta_j^0 \alpha_{jk}^0\right)}{\sum_k \left(\frac{1}{\gamma_k - 1} \sum_j \beta_j^0 \alpha_{jk}^0\right)}. \tag{5.12}$$

5.3. Examples and validations

We now examine the behavior of the Eulerian method on various test cases.

5.3.1. Advection of a discontinuity

A discontinuity of volume fraction (thus a discontinuity of the mixture density) is moving in a uniform pressure and longitudinal velocity flow at velocity 100 m/s. Initially the discontinuity is located at $x = 0.5$ m in a 1 m length tube. This discontinuity separates two nearly pure fluids, liquid water on the left with $\rho_{\mathrm{water}} = 1000\ \mathrm{kg\ m^{-3}}$, defined by the SG EOS parameters $\gamma_{\mathrm{water}} = 4.4$, $P_{\infty,\mathrm{water}} = 6 \times 10^8$ Pa and air on the right defined by $\rho_{\mathrm{air}} = 10\ \mathrm{kg\ m^{-3}}$ and the EOS parameters $\gamma_{\mathrm{air}} = 1.4$ and $P_{\infty,\mathrm{air}} = 0$ Pa. In the left chamber, the volume fraction of the water is set to $\alpha_{\mathrm{water}} = 1 - \varepsilon$ and in the right chamber its value is $\alpha_{\mathrm{water}} = \varepsilon$ ($\varepsilon = 10^{-8}$). The pressure is set uniform and equal to $P = 10^5$ Pa.

The numerical solution is plotted in Fig. 14 at time $t = 2.79$ ms and is compared to the exact one. A mesh involving 200 cells is used and a second order extension of both Lagrange and projection steps are used. Such extension is detailed in Saurel et al. [26]. The Lagrange method is used under the simplest formulation described in Section 2. No artificial heat exchange is used.

The agreement between both solutions is excellent and the solution is free of oscillations, except regarding the Mach number. This variable shows an interesting feature. As the volume fraction varies at the interface, the sound speed varies too with a non-monotonic behavior, as shown in Fig. 6. It results in important variations of the Mach number in the artificial diffusion zone of the interface. Clearly, at least one sonic point appears at the interface, even for the moderate flow velocity under interest. This puts in evidence an important feature of the Lagrange-relaxation-projection method developed herein. During the Lagrange step, there is no

need to account for the expansion fan and sonic points with the 2-shocks Riemann solver. Only the velocity and pressure at the contact discontinuity are needed. Then the projection step is done without any Riemann solver, eliminating the difficulties in the expansion fan. This is different of conventional Eulerian methods where Riemann invariants have to be solved (this is very difficult and expensive here with Relation (1.9)) or approximated. Approximating Riemann invariants when the sound speed has the non-monotonic behavior of Fig. 6 is an issue. With the present method this tricky issues are avoided, resulting in a very robust algorithm as illustrated in the next examples.

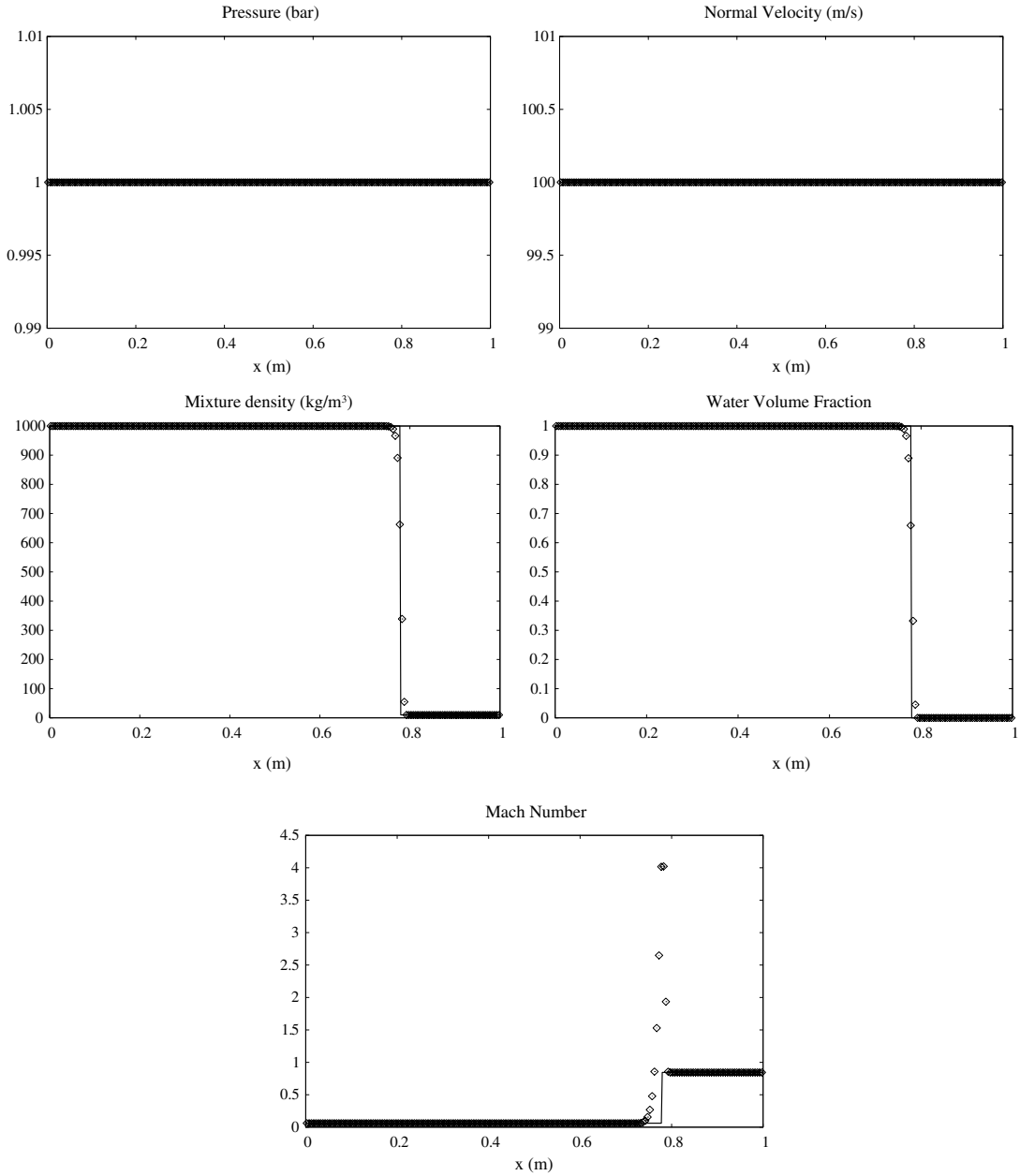

Fig. 14. Advection of a volume fraction discontinuity in a uniform pressure and velocity flow. Comparison of the Lagrange-relaxation-projection method with Superbee slope limiter (symbols) and the exact solution (solid). A 200 cells mesh is used. An excellent agreement is observed.

5.3.2. Shock tube problem with almost pure fluids

We consider in this example the single phase limit in order to check the method convergence for interface problems between pure fluids: water on the left and air on the right. The same initial data as those of Fig. 2 are used and the solution is shown at the same instant in Fig. 15. A mesh involving 1000 cells is used in order to

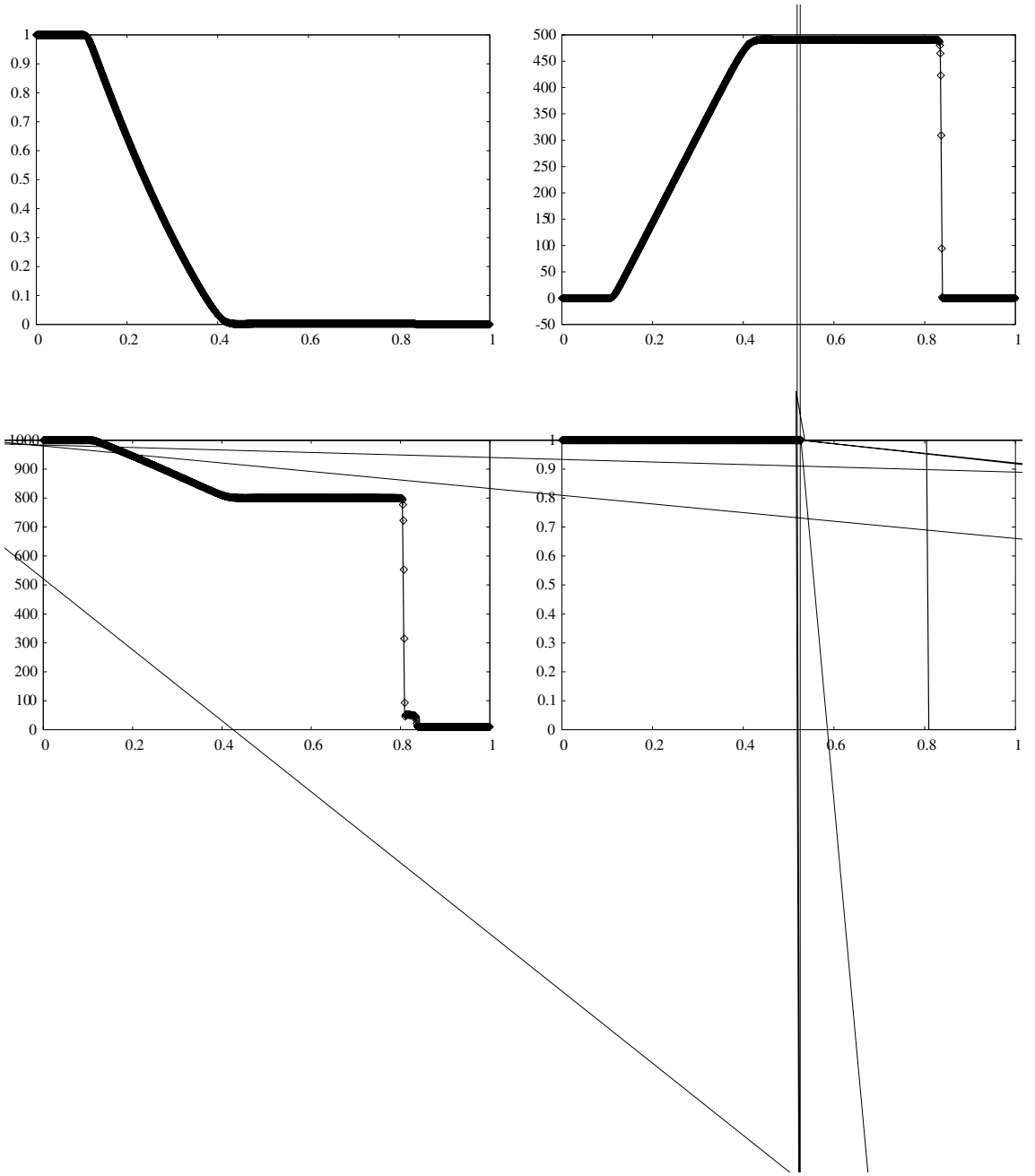

show convergence of the solution. The same algorithm as in the preceding example is used with piecewise linear reconstruction and without artificial heat exchanges. The solution is compared to the exact solution of the Euler equations.

This test clearly shows that interfaces computation with the present algorithm can be done very efficiently. The mixture remains conservative and there is no need to use artificial heat exchanges.

5.3.3. Tests with the Mie–Grüneisen (MG) equation of state

In order to show the method capabilities, in particular when dealing with more general equations of states, we now consider some tests using the MG EOS.

When dealing with such complex EOS, several modifications have to be made in the algorithm:

- The last two equations of system (1.18) are replaced by (1.17) during resolution of the Riemann problem. It means that for a given estimate of the pressure p^* a nonlinear system of two equations with the two specific volumes as unknowns has to be solved.
- An iterative resolution of system ((3.7)–(3.9)) is done instead of the direct Lagrangian cell pressure computation by (3.10).
- The relaxation-projection in the Eulerian cell is achieved with system (5.10) and (5.11) that forms a nonlinear system with seven unknowns (the cell pressure and the various specific volumes).

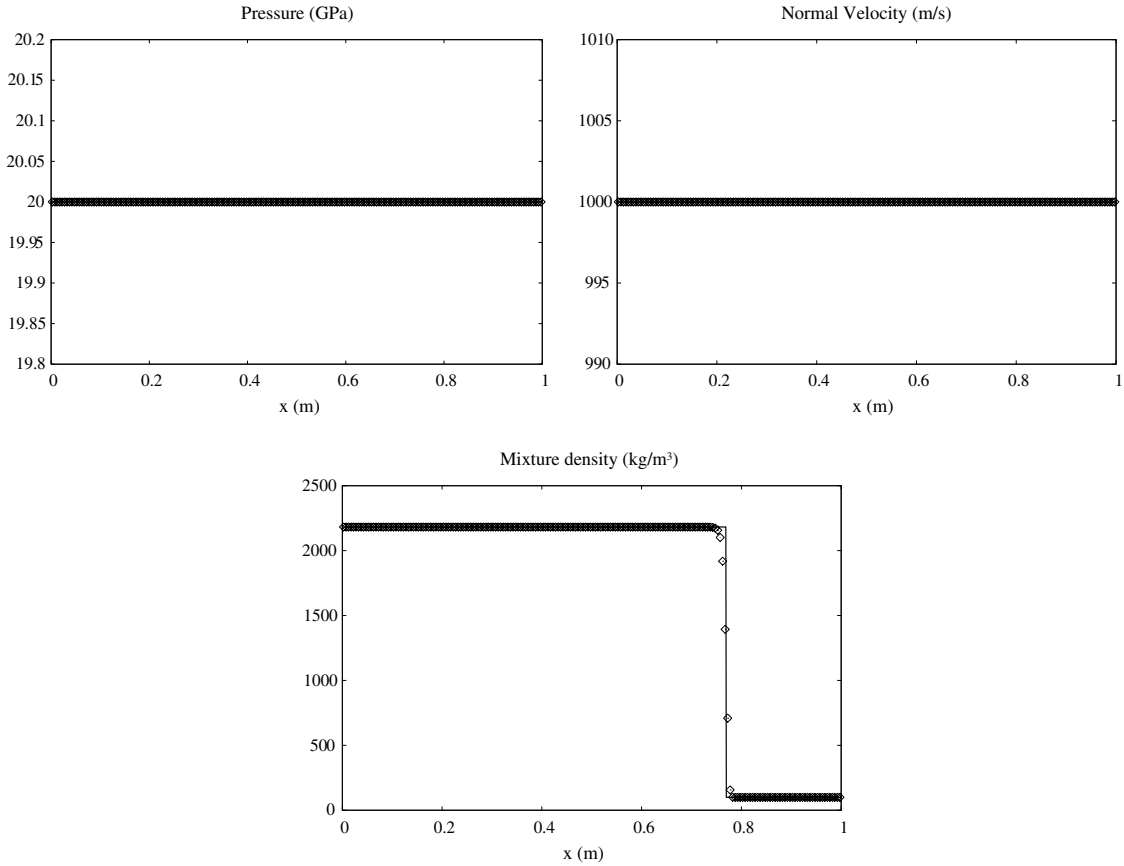

Fig. 16. Advection of a volume fraction discontinuity in a uniform pressure and velocity flow with the Mie–Grüneisen EOS. Comparison of the Lagrange-relaxation-projection method with Superbee slope limiter (symbols) and the exact solution (solid). A 200 cells mesh is used. An excellent agreement is observed.

In the first example, we consider a contact discontinuity, corresponding here to a volume fraction discontinuity moving in a uniform pressure and longitudinal velocity flow at velocity 1000 m/s and pressure of 2×10^{10} Pa. This discontinuity separates two nearly pure fluids: a real gas on the left with $\rho_{\text{gas}} = 2182\ \text{kg m}^{-3}$ and air on the right with $\rho_{\text{air}} = 100\ \text{kg m}^{-3}$. In the left chamber, the volume fraction of the real gas is set to $\alpha_{\text{gas}} = 1-\varepsilon$ and in the right chamber its value is $\alpha_{\text{gas}} = \varepsilon\ (\varepsilon = 10^{-8})$. The real gas is described by the JWL EOS [15] presented under MG form: $p(\rho,e) = \rho\Gamma(e - e_\infty(\rho)) + p_\infty(\rho)$ with

$$e_\infty(\rho) = \frac{A}{\rho_{\text{ref}}R_1}e^{-R_1\left(\frac{\rho_{\text{ref}}}{\rho}\right)} + \frac{B}{\rho_{\text{ref}}R_2}e^{-R_2\left(\frac{\rho_{\text{ref}}}{\rho}\right)} + \frac{\kappa}{\rho_{\text{ref}}\Gamma}\left(\frac{\rho_{\text{ref}}}{\rho}\right)^{-\Gamma},$$

$$p_\infty(\rho) = Ae^{-R_1\left(\frac{\rho_{\text{ref}}}{\rho}\right)} + Be^{-R_2\left(\frac{\rho_{\text{ref}}}{\rho}\right)} + \kappa\left(\frac{\rho_{\text{ref}}}{\rho}\right)^{-(\Gamma+1)}.$$

The different constants involved in these relations are:

$$\kappa = \left[p_{CJ} - Ae^{-R_1\left(\frac{\rho_{\text{ref}}}{\rho_{CJ}}\right)} - Be^{-R_2\left(\frac{\rho_{\text{ref}}}{\rho_{CJ}}\right)} - \rho_{CJ}\Gamma C_v T_{CJ}\right]\left(\frac{\rho_{\text{ref}}}{\rho_{CJ}}\right)^{\Gamma+1}.$$

The data used in the present simulations are: $\Gamma = 0.35$, $A = 353.91\times10^9$ Pa, $B = 3.45\times10^9$ Pa, $R_1 = 4.15$, $R_2 = 0.9$, $C_v = 815$ J/kg/K, $\rho_{\text{ref}} = 1590\ \text{kg/m}^3$, $\rho_{\text{CJ}} = 2182\ \text{kg/m}^3$, $p_{\text{CJ}} = 2\times10^{10}$ Pa, $T_{\text{CJ}} = 3686$ K.

Air is described by the SG EOS with parameters $\gamma_{\text{air}} = 1.4$ and $P_{\infty,\text{air}} = 0$ Pa.

The discontinuity is initially located at $x = 0.5$ m. Results are presented in Fig. 16 at time $t = 270$ μs.

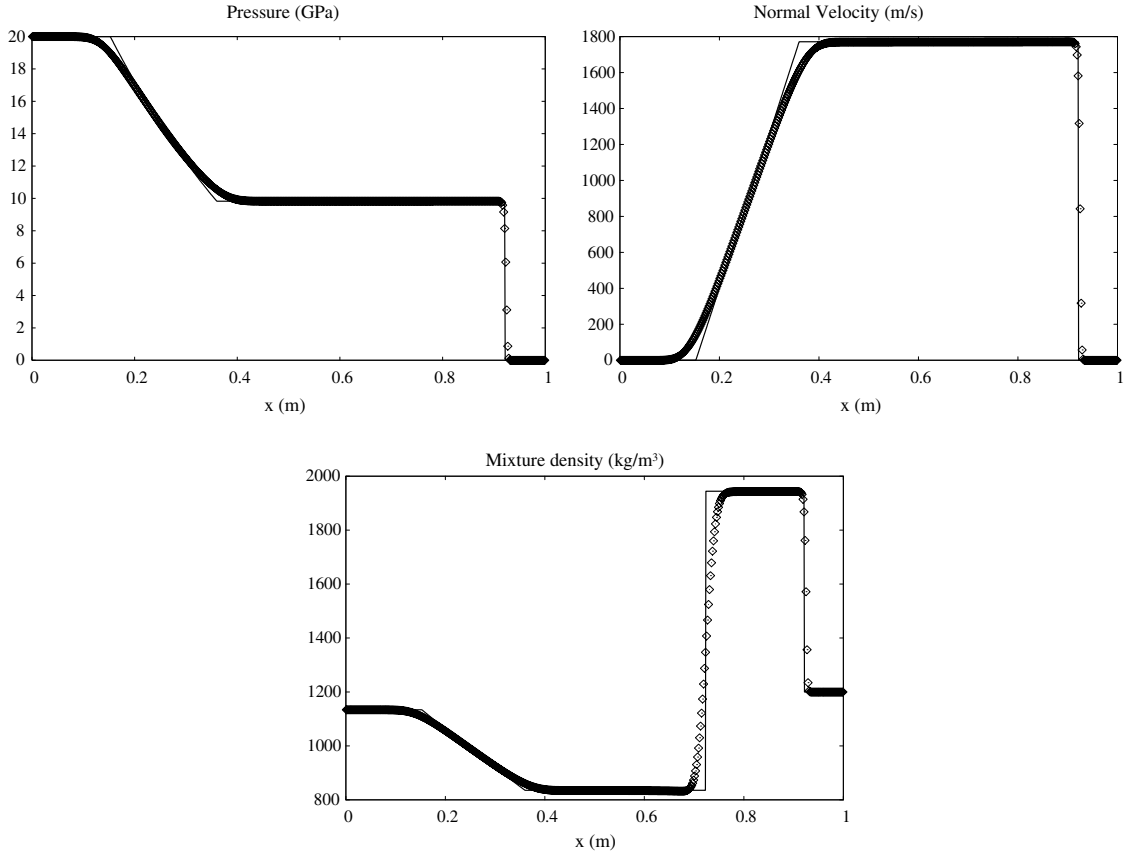

Fig. 17. Shock tube with Mie–Grüneisen EOS. The Lagrange-relaxation-projection method (symbols) is compared to the exact solution of the Euler equations (solid). A 500 cells mesh is used. Results are in correct agreement.

The second example is the shock tube problem with the MG EOS presented in Saurel et al. [26], in Section 3. In this test case, a single fluid governed by the Cochran–Chan [7] EOS is considered. This EOS is also of MG type. As there is a single fluid, the Godunov method is expected to work. However, it was shown in Saurel et al. [26] that due to the nonlinearity of $p_\infty(\rho)$ in the EOS, the Godunov method was producing pressure and velocity oscillations. A cure to these difficulties was proposed in the same reference. Here, with the help of the multiphase flow model, these difficulties can be solved by considering the single MG fluid as a two-phase media, the initial discontinuity in the shock tube separating the two phases.

Initially, the high pressure chamber is set to 2×10^{10} Pa, while the pressure is set equal to 2×10^{5} Pa in the low pressure chamber. Both chambers are filled with two phases of liquid nitromethane, governed by the MG EOS which densities are respectively set to 1134 kg/m^3 and 1200 kg/m^3. In the high pressure chamber, volume fraction of the first phase is set to $\alpha_1 = 1-\varepsilon$ and in the right chamber its value is $\alpha_1 = \varepsilon$ ($\varepsilon = 10^{-8}$). Then, the model is used in the single phase limit. All details regarding the EOS and initial data are given in Saurel et al. [26]. Solution is presented at time $t = 70$ μs in Fig. 17. The Lagrange-relaxation-projection method is compared to the exact solution of the Euler equations. Results are similar to those of Saurel et al. [26] with the correction used in the projection stage of the solution onto the Eulerian grid. A magnified view of pressure and velocity around the contact discontinuity is given in Fig. 18. It presents a solution free of oscillations.

5.3.4. Shock tube problem with mixtures of materials with the Eulerian method

We now consider the shock tube test problem with mixtures of materials with the same initial data as those of Figs. 3, 5, 7, 10 and 11. The numerical solution is shown in Fig. 19 and compared with the exact solution at time $t = 29$ μs.

Numerical solution and exact one are in excellent agreement. However, it is worth to mention that the Eulerian method does not present the same artificial shock smearing as the pure Lagrangian method used in Fig. 10. Consequently, the heat exchange function μ has to be rebuilt. The procedure described in Section 4.3 is reused with the Eulerian algorithm of the present section. The corresponding $\bar{\mu}$ function is shown in Fig. 20.

5.3.5. Two-dimensional example

The aim is to show the ability of the method to deal with multi-dimensional and multi-phase simulations involving complex equations of states. In 1D the solution is computed in two steps which can be summarized as follows:

$$U_i^{n+1} = L_{X,\Delta t}(U_i^n),$$

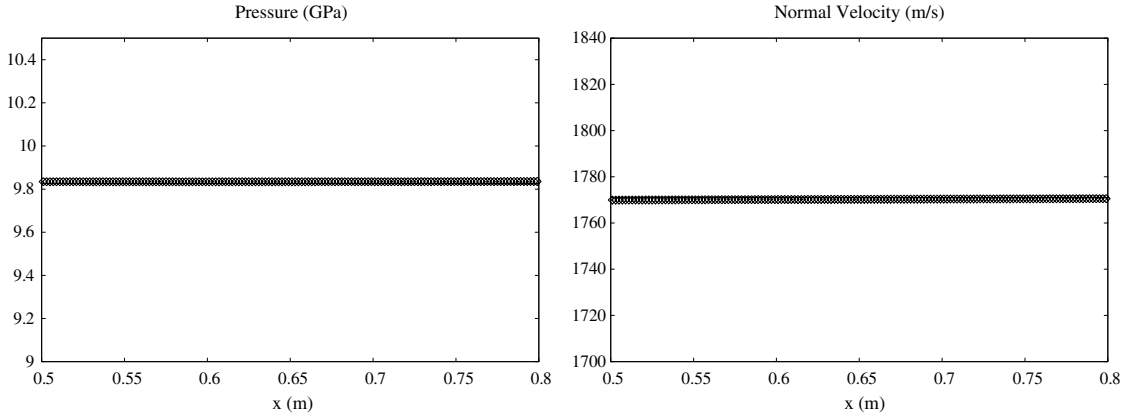

Fig. 18. Shock tube with Mie–Grüneisen EOS. Magnified view of pressure and density around the contact discontinuity. Results are in perfect agreement with the exact solution and solution is free of oscillations.

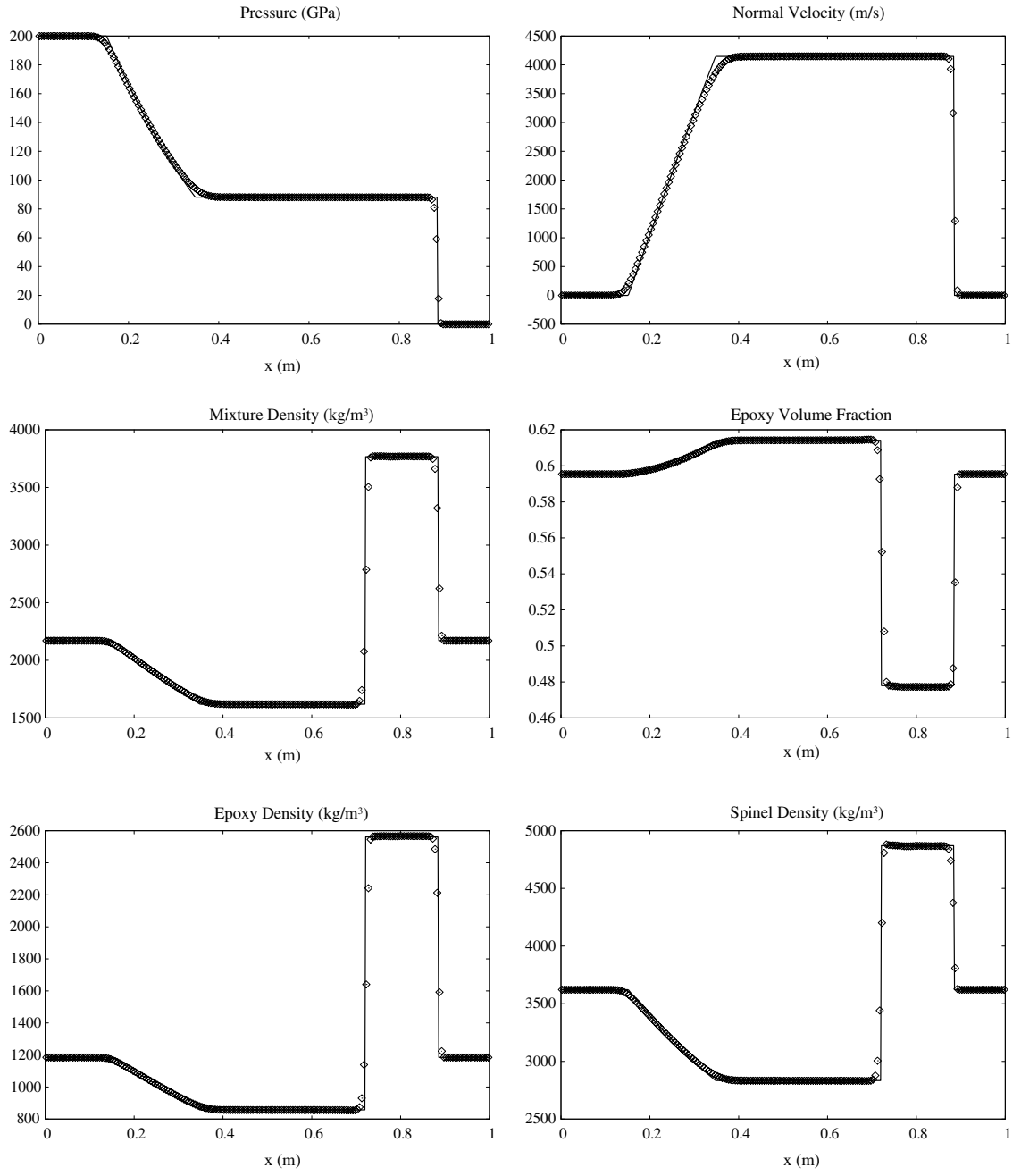

Fig. 19. Epoxy–spinel shock tube. The Lagrange-relaxation-projection method (symbols) is compared to the exact solution (solid). A second order version of the Lagrange method is used with Van Leer slope limiter and with artificial heat exchanges in the shock layer. The relaxation-projection method of Saurel et al. [26] is used to project the solution on the Eulerian grid with piecewise linear functions based on Superbee slope limiter. A 200 cells mesh is used.

where $L_{X,\Delta t} = L_{\text{Projection}} L_{\text{Lagrange}}$ is the succession of the Lagrangian step, which computes the solution in the Lagrangian cells and of the relaxation-projection step, which projects the solution onto the Eulerian grid.

In multi-dimensional case a splitting strategy was used [31]. Thus, the solution is computed by:

$$U_i^{n+2} = L_{X,\Delta t} L_{Y,\Delta t} L_{Y,\Delta t} L_{X,\Delta t}(U_i^n).$$

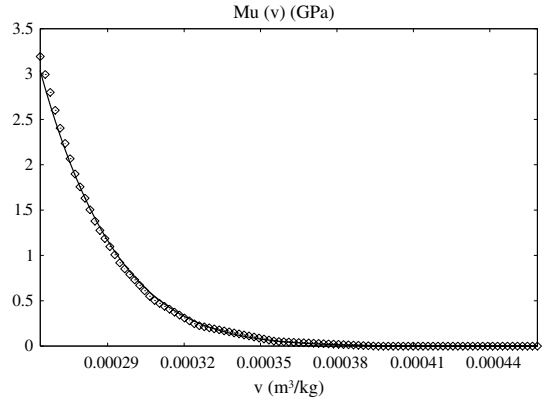

Fig. 20. New values of the heat exchange function μ for the Lagrange-relaxation-projection method (symbols) and fitting curve ($\bar{\mu}(v) = \exp[-1.04 \times 10^8 \times v^2 + 2.12 \times 10^4 \times v + 23.4]$) in the specific volume range (2.65×10^{-4}–4.61×10^{-4} m^3/kg) corresponding to a piston velocity range of 0–4200 m/s and a pressure range of 1–880,000 atm.

In order to illustrate the capabilities of the method, we consider a two-dimensional test dealing with impact of a projectile on a tank containing two different fluids. The initial configuration is detailed in Fig. 21. This problem involves four fluids: air, copper, real gas (RG) and liquid nitromethane (NM). Air and copper are governed by the SG EOS. The parameters for the copper are $\gamma_{\text{copper}} = 4.22$ and $P_{\infty,\text{copper}} = 324 \times 10^8$ Pa. The real gas is described by the JWL EOS used in the example of Fig. 16 while the liquid nitromethane obeys the Cochran–Chan EOS used in the example of Fig. 17. Initially, densities of each fluid are: $\rho^0_{\text{air}} = 1$ kg/m^3, $\rho^0_{\text{copper}} = 9000$ kg/m^3, $\rho^0_{\text{RG}} = 1590$ kg/m^3 and $\rho^0_{\text{NM}} = 1134$ kg/m^3. The projectile impacts the tank at the velocity of 10 km/s.

We can see that this test involves strong densities ratios (of the order of 10^4), four different EOS with two complex ones, and very strong shocks due to the velocity of the projectile. Results are shown in Fig. 22 at different times.

It is interesting to note the ability of the method to predict the 'cavitation' effect that appears in the projectile. Due to multi-dimensional dynamics of expansion waves, the projectile is over expanded after shock loading. It results in a vacuum pocket that dynamically appears in the projectile, forming a solid shell on the left part of it. Shell formation is a well-known phenomena in the physics of high velocity impacts [32]. The present method is able to deal with the dynamic appearance of interfaces.

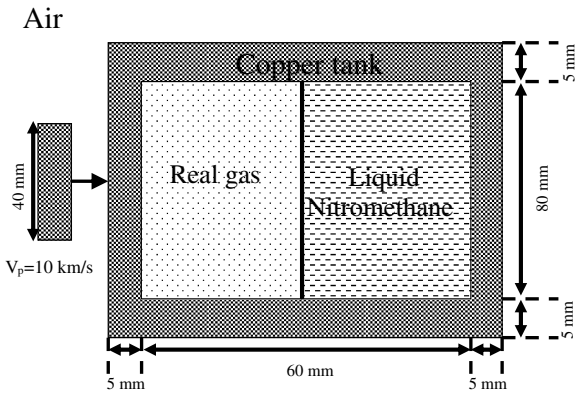

Fig. 21. Schematic view of the two-dimensional test. A copper projectile impacts a copper tank surrounded by air and filled with a real gas and liquid nitromethane. Both copper and air are governed by the SG EOS. The real gas is described by the JWL EOS used in the example of Fig. 16 while the liquid nitromethane obeys the Cochran–Chan EOS used in the example of Fig. 17.

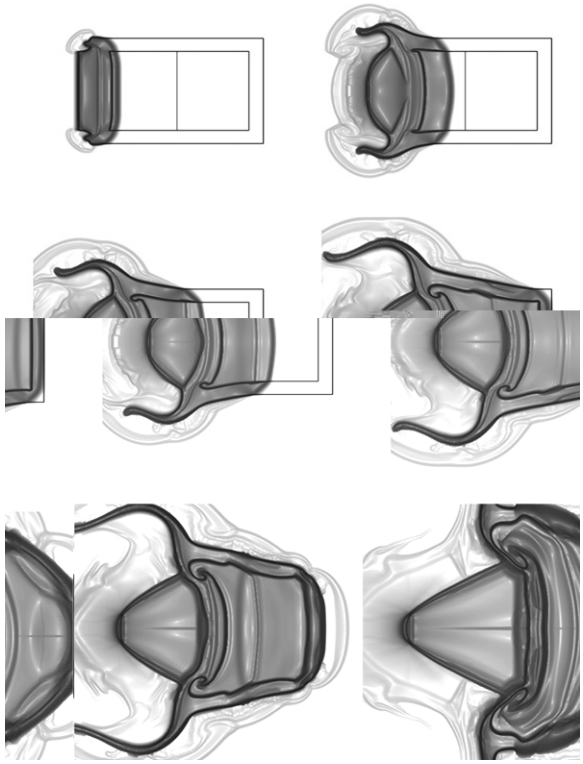

Fig. 22. Impact of a projectile on a tank containing two fluids. Mixture density gradients are shown at times 11, 33, 52, 81, 102 and 193 μs. A 500×500 cells mesh is used. The method treats without difficulty the presence of multiple interfaces.

6. Conclusion

The relaxation-projection method developed in Saurel et al. [26] is extended to the non-conservative hyperbolic multiphase flow model of Kapila et al. [13]. The non-conservative character of this model poses however computational challenges in the presence of shocks. Thanks to the Rankine–Hugoniot relations proposed in Saurel et al. [27] exact and approximate 2-shocks Riemann solvers are derived. But an important difficulty appears for the computation of the correct energy partition between phases under strong shocks in cell average states. To circumvent this difficulty a specific Lagrangian scheme is developed. The correct partition of the energies is reached by using an artificial heat exchange in the shock layer. With the help of an asymptotic analysis this heat exchange takes a differential form that can be used in the shock layer only. The Lagrangian scheme thus combines Riemann solvers and artificial heat exchanges. An Eulerian variant is then obtained by using the relaxation-projection method developed earlier [26]. The method is validated against exact solutions based on the multiphase shock relations as well as exact solutions of the Euler equations in the context of interface problems. The method is able to solve interfaces separating pure fluids or heterogeneous mixtures with very large density ratios and with very strong shocks.

Acknowledgments

This work was partially supported by DGA Centre d'Etudes de Gramat. The authors are particularly grateful to Dr. Gérard Baudin. They also address special thanks to Professor Sergey Gavrilyuk of the SMASH Project.

References

[1] R. Abgrall, How to prevent pressure oscillations in multicomponent flow calculations: a quasi conservative approach, J. Comput. Phys. 125 (1996) 150–160.

[2] R. Abgrall, R. Saurel, Discrete equations for physical and numerical multiphase mixtures, J. Comput. Phys. 186 (2) (2003) 361–396.
[3] R. Abgrall, V. Perrier, Asymptotic expansion of a multiscale numerical scheme for compressible multiphase flows, SIAM J. Multiscale Model. Simul. (5) (2006) 84–115.
[4] G. Allaire, S. Clerc, S. Kokh, A five equation model for the simulation of interfaces between compressible fluids, J. Comput. Phys. 181 (2) (2002) 577–616.
[5] M.R. Baer, J.W. Nunziato, A two-phase mixture theory for the deflagration-to-detonation transition in reactive granular materials, Int. J. Multiphase Flows 12 (1986) 861–889.
[6] A. Chinnayya, E. Daniel, R. Saurel, Computation of detonation waves in heterogeneous energetic materials, J. Comput. Phys. 196 (2004) 490–538.
[7] G. Cochran, J. Chan, Shock initiation and detonation models in one and two dimensions, CID-18024 Lawrence National Laboratory Report, 1979.
[8] R. Courant, K.O. Friedrichs, Supersonic flow and shock waves, in: Applied Mathematical Sciences, vol. 21, Springer Verlag, 1948.
[9] O. Coutier-Delgosha, R. Fortes-Patella, J.L. Reboud, N. Hakimi, C. Hirsch, Stability of preconditioned Navier–Stockes equations associated with a cavitation model, Comput. Fluids 34 (2005) 319–349.
[10] R. Fedkiw, T. Aslam, B. Merriman, S. Osher, A nonoscillatory Eulerian approach to interfaces in multimaterial flows (the ghost fluid method), J. Comput. Phys. 152 (1999) 457–492.
[11] J. Glimm, J.W. Grove, X.L. Li, K.M. Shyue, Y. Zeng, Q. Zhang, Three dimensional front tracking, SIAM J. Sci. Comp. 19 (3) (1998) 727–783.
[12] S.K. Godunov, A. Zabrodin, M. Ivanov, A. Kraiko, G. Prokopov, Résolution numérique des problèmes multidimensionnels de la dynamique des gaz, Mir, Moscow, 1979 (in French).
[13] A.K. Kapila, R. Menikoff, J.B. Bdzil, S.F. Son, D.S. Stewart, Two-phase modeling of deflagration to detonation transition in granular materials: reduced equations, Phys. Fluids 13 (10) (2001) 3002–3024.
[14] S. Karni, Multicomponent flow calculation by a consistent primitive algorithm, J. Comput. Phys. 112 (1994) 31–43.
[15] E.L. Lee, H.C. Horning, J.W. Kury, Adiabatic expansion of high explosives detonation products, Lawrence Radiation Laboratory, University of California, Livermore, TID 4500-UCRL 50422, 1968.
[16] O. Le Metayer, J. Massoni, R. Saurel, Modeling evaporation fronts with reactive Riemann solvers, J. Comput. Phys. 205 (2005) 567–610.
[17] R.J. LeVeque, K.M. Shyue, One-dimensional front tracking based on high resolution wave propagation methods, SIAM J. Sci. Comp. 16 (2) (1995) 348–377.
[18] S.P. Marsh, LASL Shock Hugoniot Data, University of California Press, 1980.
[19] J. Massoni, R. Saurel, G. Demol, G. Baudin, A Mechanistic model for shock to detonation transition in solid energetic materials, Phys. Fluids 11 (3) (1999) 710–736.
[20] J. Massoni, R. Saurel, B. Nkonga, R. et Abgrall, Proposition de méthodes et modèles eulériens pour les problèmes à interfaces entre fluides compressibles en présence de transfert de chaleur, Int. J. Heat Mass Transfer 45 (6) (2002) 1287–1307 (in French).
[21] A. Murrone, H. Guillard, A five equations reduced model for compressible two-phase flow problems, J. Comput. Phys. 202 (2004) 664–698.
[22] G. Perigaud, R. Saurel, A compressible flow model with capillary effects, J. Comput. Phys. 209 (2005) 139–178.
[23] R. Saurel, R. Abgrall, A multiphase Godunov method for compressible multifluid and multiphase flows, J. Comput. Phys. 150 (1999) 425–467.
[24] R. Saurel, O. Le Metayer, A multiphase model for interfaces, shocks, detonation waves and cavitation, J. Fluid Mech. 431 (2001) 239–271.
[25] R. Saurel, S. Gavrilyuk, F. Renaud, A multiphase model with internal degree of freedom: application to shock–bubble interaction, J. Fluid Mech. 495 (2003) 283–321.
[26] R. Saurel, E. Franquet, E. Daniel, O. Le Metayer, A relaxation-projection method for compressible flows. Part I: The numerical equation of state for the Euler equations, J. Comput. Phys. (2007) 822–845.
[27] R. Saurel, O. Le Metayer, J. Massoni, S. Gavrilyuk, Shock jump conditions for multiphase mixtures with stiff mechanical relaxation, Shock Waves 16 (3) (2007) 209–232.
[28] R. Saurel, F. Petitpas, R. Abgrall, Modelling phase transition in metastable liquids, J. Fluid Mech. (submitted).
[29] E. Sinibaldi, Implicit preconditioned numerical schemes for the simulation of three-dimensional barotropic flows, Ph.D. Thesis, Scuola Normale Superiore di Pisa, Italy, 2006.
[30] K.M. Shyue, An efficient shock-capturing algorithm for compressible multicomponent problems, J. Comput. Phys. 142 (1998) 142.
[31] G. Strang, On the construction and comparison of difference schemes, SIAM J. Numer. Anal. 5 (3) (1968) 506–517.
[32] J. Thouvenin, Détonique, CEA Eyrolles, Paris, 1997 (in French).
[33] E.F. Toro, Riemann Solvers and Numerical Methods for Fluids Dynamics, Springer, Berlin, 1997.
[34] R.F. Trunine, Shock compression of condensed materials (laboratory studies), Phys. Usp. 44 (2001) 371.
[35] E.H. Van Brummelen, B. Koren, A pressure invariant conservative Godunov-type method for barotropic two-fluid flows, J. Comput. Phys. 185 (2003) 289–308.
[36] J. Von Neumann, R.D. Richtmyer, A method for the numerical calculation of hydrodynamic shocks, J. Appl. Phys. 21 (1950) 232–237.
[37] A.B. Wood, A Textbook of Sound, G. Bell and Sons LTD, London, 1930.